Mineralogical Magazine, June 2003, Vol. 67(3), pp. 423–451

The Turiy Massif, Kola Peninsula, Russia: mineral chemistry of an ultramafic-alkaline-carbonatite intrusion

E. A. DUNWORTH*,† AND K. BELL

Ottawa-Carleton Geoscience Centre, Department of Earth Sciences, Carleton University, Ottawa, Ontario, K1S 5B6 Canada

ABSTRACT

The Turiy Massif, on the southern coast of the Kola Peninsula, consists of five intrusive complexes containing a variety of carbonatites, phoscorites, melilitolites, ijolites and pyroxenites. Petrographic and mineralogical studies of the different rocks show that the samples are texturally heterogeneous. Minerals including apatite, garnet, magnetite, melilite, mica and pyroxene, show systematic variations in composition relating to the rock type in which they occur. Compositional similarities and/or distinct trends are seen in the mineral compositions within the each of the pyroxenite-melilitolite, and melteigite-ijolite rock series, indicating linked petrogenetic histories within each of the two series. The carbonatites from the northern complex may be related to nearby melilitolites, but the central complex carbonatites and phosocorites do not bear any mineralogical (or isotopic) similarities to any of the silicate rocks within the massif.

KEYWORDS: carbonatite, phoscorite, melilitolite, ijolite, pyroxenite, mineral chemistry, Turiy Massif, Kola Peninsula, Russia.

Introduction

THE Kola Peninsula, located between ~66–70ºN and ~30–42ºE in northwestern Russia, bounded by the White Sea and Kandalaksha Graben to the south, and the Barents Sea to the north, is underlain by Archaean gneisses and granite-gneisses. It contains ~25 Palaeozoic alkaline intrusions whose emplacement was largely controlled by pre-existing, reactivated, lithospheric fractures including the Kontozero Graben and Kandalaksha Deep Fracture Zone (Kogarko *et al.*, 1995). The alkaline massifs range in size from 1–40 km in diameter, and in composition from pyroxenite-olivinite (e.g. Afrikanda) to ijolite-melilitolite-carbonatite (e.g. Turiy, Kovdor) and ijolite-syenite-carbonatite (e.g. Khibina). Most consist of sub-vertical pipes and stocks, commonly containing ring dyke or cone sheet intrusions. A Rb-Sr isochron study of several of these Kola massifs suggests that most are Upper Devonian in age (Kramm *et al.*, 1993).

The Turiy Massif, located on the south coast of the Kola Peninsula, mid-way along the Kandalaksha Graben, is part of a small peninsula jutting out into the White Sea. With a total area of ~50 km^2, the massif is mostly covered by 30 m of glacial till and surficial material (Ronenson *et al.*, 1981), and is exposed only along the shore-line on the western coast. The probable original level of emplacement of the massif was 1–2 km, i.e. a confining pressure of ~5 kbar; the current depth to the base of the massif, based on geophysical evidence, is 3–5 km (Bulakh and Ivanikov, 1984).

A geological map of the Turiy Peninsula (Fig. 1), based on detailed studies of drill core material (Ronenson *et al.*, 1981) outlines five intrusive/hypabyssal centres, each containing a variety of rock types. A central complex (28 km^2) is surrounded by satellite complexes to the north (~1 km^2), south (13 km^2), east (10 km^2), and the Kuznavalok complex to the west (1.3 km^2). The latter contains the type-locality for the rock-type

* E-mail: lizzyann@magma.ca
DOI: 10.1180/0026461036730109
† Meridian Scientific Services Inc., Box 1150, 2458 Huntley Rd, Stittsville, Ontario, K2S 1B8 Canada

© *2003 The Mineralogical Society*

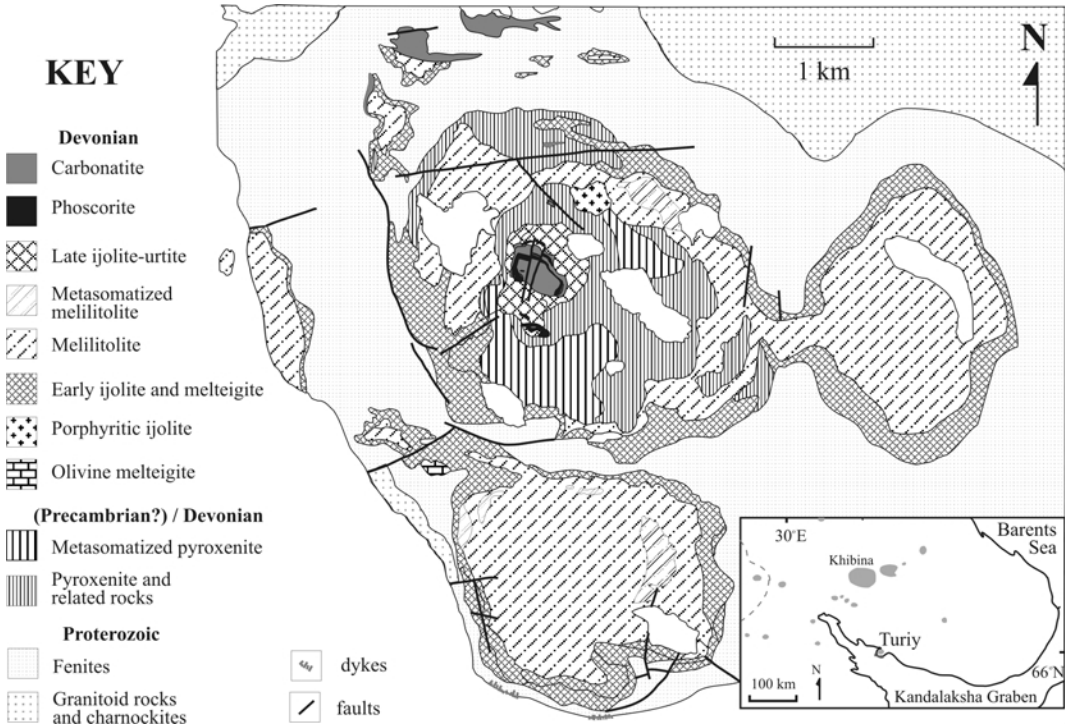

FIG. 1. Map of the Turiy Peninsula (after Ronenson *et al.*, 1981) showing the five main complexes and south-coast dyke swarms. The massif is exposed only on the west coast. Inset: Map of the Kola Peninsula showing the location of Palaeozoic alkaline intrusions (after Bell *et al.*, 1996). KH = Khibina, L = Lovozero, T = Turiy, K = Kandalaksha.

turjaite, which crops out on the western shore and shows banding and layering typical of a convecting and crystallizing magma body. The northern complex represents a suite of small, scattered bodies, as seen in Fig. 1. Several dyke swarms occur in the south and south-west coast of the peninsula. They form three intrusive phases, that are pre-, syn- and post-emplacement relative to the massif (Bulakh and Ivanikov, 1984). The massif itself was emplaced into Proterozoic charnockites which are overlain by Riphean sandstones along the south coast of the Turiy Peninsula (Bulakh and Ivanikov, 1984; Kogarko, 1987). A 500–700 m wide fenitized aureole surrounds the massif. For further information, and a detailed description of the two type-locality rocks, turjaite and turjite, the reader is referred to Bell *et al.* (1996) and references therein.

Rock types

On the basis of detailed petrographic studies by Ronenson *et al.* (1981), Bulakh and Ivanikov (1984, 1996) and this work, the nomenclature of the Turiy rocks has been revised according to the IUGS classification of igneous rocks (Le Maitre, 1989), and the melilitolite classification of Dunworth and Bell (1998). Thus, the Turiy complex includes pyroxenites, melteigite-ijolite-urtites, melilitolites, phoscorites and carbonatites. The modal mineralogy of a representative suite of samples examined in this study is shown in Table 1, although this should be considered a general guide to the petrography of the complex given the extreme textural variablity and heterogeneity shown by most of the drill-core material and outcrops. Each of these rock types will be discussed in turn.

Pyroxenites

Pyroxenites are found only in the central complex, and consist of pale yellow/green, medium- to coarse-grained, equigranular, anhedral to subhedral clinopyroxene. Interstitial accessory minerals include amphibole, apatite,

calcite, garnet, magnetite, nepheline and perovskite. The anhedral cores of many pyroxenes from one sample [C.AG.347] contain euhedral exsolution lamellae of chrome spinel, while diopsidic overgrowths around the cores suggest adcumulate growth.

Melilitolites

One of two type-locality rocks at Turiy, the melilitolite known as 'turjaite', occurs in all five complexes in the massif. Turjaite was originally defined as an intrusive melilite-nepheline rock, with accessory phlogopite, magnetite, perovskite, apatite and calcite (Ramsay, 1921). A number of additional accessory minerals have been found in the turjaite samples examined in this study (Table 1) (Bell *et al.*, 1996). Ronsenson *et al.* (1981) and Bulakh and Ivanikov (1996) report rare uncompahgrites (pyroxene melilitolites) and olivine melilitolites within the central complex, as well as melilitolites rich in perovskite and magnetite, similar to the melilitolites of the Gardiner Complex in Greenland (Nielsen, 1980). Calcite melilitolites grading into melilite-calcite carbonatites have been found in Turiy's northern complex, similar to those found at Oka (Treiman and Essene, 1985).

Ijolite series

On the basis of findings from drill-core material, Bulakh and Ivanikov (1984) suggested that there are two temporally and geographically distinct suites of ijolite-series rocks within the Turiy massif. One is more mafic and pyroxene-rich, and forms an outer ring around all the ultramafic complexes (Fig. 1) (Ronenson *et al.*, 1981), similar to those found at Kovdor, Poschni, Vuoriyarvi and several other massifs within the Kola Peninsula (Borodin, 1963; Kapustin, 1980). The second, more leucocratic ijolite series at Turiy, encloses the main carbonatite-phoscorite stock within the central complex.

Most samples from both ijolite series are medium- to coarse-grained, relatively texturally homogeneous, and rich in pale green diopsidic pyroxene, nepheline and melanite garnet. Garnet and tetra-ferriphlogopite replace pyroxene in the central complex samples. Apatite, magnetite, ilmenite, perovskite and titanite also occur, although the Fe oxide phases are rare. Calcite, banalsite, stronalsite, analcime, pectolite, sodalite and wollastonite occur as accessory minerals in some samples, and zeolites and cancrinite are common alteration products.

A hypabyssal, porphyritic olivine melteigite pipe on the eastern edge of the central complex contains abundant, coarse-grained, rounded olivine and green-brown, inclusion-rich, zoned, augite phenocrysts. K-poor nepheline forms most of the groundmass, poikilitically enclosing rare, euhedral and fine-grained aegirine crystals.

Phoscorites

Phoscorites only occur in the central complex, and form arcuate bodies within the central parts of the carbonatite stock (Fig. 1). They are believed to have been intruded after the second suite of ijolites and prior to the carbonatites (Bulakh and Ivanikov, 1984). Their proposed origin as hydrothermal veins (Kukharenko, 1965) is unlikely at Turiy, given their extremely depleted Sr-Nd isotopic signatures and magmatic $\delta^{18}O$-$\delta^{13}C$ signatures (Dunworth and Bell, 2001).

The mineralogy of the phoscorites is dominated by magnetite, phlogopite, apatite and calcite, along with pyroxene, sulphides and other accessory minerals. All phlogopites from the Turiy phoscorite samples examined in this study show a vivid orange pleochroism, and reverse absorption; concentric zoning and resorption effects are common. Apatite occurs both as monomineralic veins within the samples and as interlocking grains with magnetite. Because monomineralic clusters and/or veins are common in these samples, it is difficult to obtain accurate estimates of their modal mineralogy. Although forsterite was not found in any of the samples in this study, it has been reported in other phoscorites from Turiy (Bulakh and Ivanikov, 1984) and is a common component of the Kovdor and Vuoriyarvi phoscorites (Kapustin, 1980).

Carbonatites

Most of the Turiy carbonatites, extremely variable in both modal mineralogy and chemical composition, occur within the middle part of the central complex and as scattered outcrops within the northern complex. Most are calcite carbonatites with accessory apatite, phlogopite and magnetite. Given the textural heterogeneity within the limited size of the drill-core samples studied, we have included samples with >40% carbonate minerals within the carbonatite group in

TABLE 1. Modal mineralogy of a suite of samples from a variety of rock types. The initial letter of each sample number indicates from which complex the sample is taken (N = north, E = east, S = south, W = west, C = central).

	Pyroxenite-melteigite-ijolite-urtite series					Turjite*
Complex	C	C	C	C	C	
Sample	AG.347	AG.48A	AG.122	ND.500	IJ.14	TQ
Rock type	Pyxite	Ol. melt.	Melteigite	Ij. (1)	Ij. (2)	
Amphibole	8					
Analcime			<1			
Apatite	<1	2		3	3	
Banalsite			<1		<1	
Calcite	1	<1	2	2		
Cancrinite			2			
Chromite	1					
Garnet	1		13	5	25	
Ilmenite					<1	
Magnetite	10	3		3	2	
Mica		3	1	2	5	
Nepheline		6	18	55	52	
Olivine		38				
Pectolite					1	
Perovskite	8	1	<1		<1	
Pyroxene	70	55	62	25	5	
Sodalite					2	
Sulphides			1			
Titanite		1				
Wollastonite					4	
Zeolites		1		5		

Analcime						
Apatite						
Calcite	8					
Cancrinite						
Celsian						
Garnet	10					
Ilmenite						
Magnetite	5					
Melilite (?)	37					
Mica	18					
Perovskite	<1					
Pyroxene						
Strontianite						
Titanite	<1					

	Melilitolites*				Other rock types		
Complex	N	C	C	Complex	South coast		
Sample	64.18	190.105	5.118	Sample	TD 1	TD 2	NC.153.82
Rock type	Cal mel.	Turjaite	Mica turjaite	Rock type	Late-stage veins		Fenite
Apatite			1	Alteration			10
Calcite	28	<1		Amphibole			8
Garnet	1	3	2	Ankerite	20	5	
Magnetite	10	5	3	Apatite	5	30	<1
Melilite	55	40	46	Baryte		<1	1
Mica	2	12	22	Calcite	35	15	3
Monticellite	1			Feldspar		10	59
Nepheline		35	23	Fluorite	30		
Perovskite	2	5	3	Mica		1	
Pyroxene	<1			Pyroxene		40	15
Sulphides	1			Quartz	9		
Wollastonite	?			Rutile	<1	<1	
				Strontianite		<1	
				Sulphides	1		<1
				Titanite			<1
				Wollastonite			<1
				Zircon			<1

Rock-type abbreviations: Pyxite = pyroxenite; Melt. = melteigite; Ij. = ijolite; mel. = melilitolite
* modal mineralogy of type-locality samples also given in Bell *et al.* (1996)
(1) = 1st ijolite series
(2) = 2nd ijolite series
Modal mineralogy estimates based on thin-section point-counting
Alteration = unidentified alteration products

TABLE 1 (*contd.*)

	Central complex carbonatites							
Complex	C	C	C	C	C	C	C	C
Sample	TL.344	6.15	49.40	54.x	100.a	100.b	100.y	DC
Amphibole	5						6	
Apatite	29	17	22	4	3	4	2	4
Baddelyite		1						
Baryte								
Calcite	40	40	43	52	55	84	78	46
Chlorite						<1	<1	
Dolomite		5	5		34		3	46
Garnet				15				
Ilmenite	3	3				<1	<1	
Magnetite	15	26	12			5	6	
Mica	4	8	18	20	5	4	3	
Perovskite	<1			2				
Pyrochlore							<1	
Pyroxene	4							
Strontianite				<1		<1	<1	
Sulphides					3	2		3
Zeolites				7				
Zircon							<1	
Zirsinalite								

	Northern complex carbonatites				Phoscorites		
Complex	N	N	N	Complex	C	C	C
Sample	64.19	63	187.100	Sample	K.7	19.2	3.93
Apatite	<1	<1	1	Amphibole	1		4
Calcite	70	47	55	Apatite	<1	10	1
Garnet	1	1	7	Calcite	27	18	58
Ilmenite			<1	Chlorite		<1	1
Magnetite	2	2	1	Dolomite		2	
Melilite	6			Ilmenite	<1	1	
Mica	11	2	17	Magnetite	28	47	8
Monticellite	10			Mica	30	22	28
Quartz			3	Perovskite			
Perovskite	?			Pyroxene	10		
Pyroxene		48	15	Strontianite		<1	
Titanite			<1	Sulphides	3		
				Unknown			
				Zircon		<1	

Table 1, contrary to the standard definition of >50% (Le Maitre, 1989). Textural heterogeneity includes bands, veins and variations in grain size both within and between samples. Sample C.6.15, as one example, contains apatite-magnetite bands of variable thickness and grain size, separated by bands of calcite and dolomite (Fig. 2*a*). One magnetite-apatite band shows the development of baddeleyite rims around the apatite grains, a feature not seen in neighbouring magnetite-apatite veins. Apatite veins are enclosed within natrolite in sample C.54.x, a late-stage calcite-natrolite carbonatite vein (Fig. 2*b*).

Two small satellite bodies in the northern complex contain SiO_2-rich carbonatites ($\geqslant 10\%$ SiO_2) with low apatite and magnetite contents. Several samples contain up to 40% garnet + pale green/brown phlogopite + pyroxene. Those carbonatites that lack pyroxene are melilite-bearing, including one sample that also contains ~10% monticellite. Sample N.187.134 exhibits rare rounded calcite grains ~3 mm in diameter,

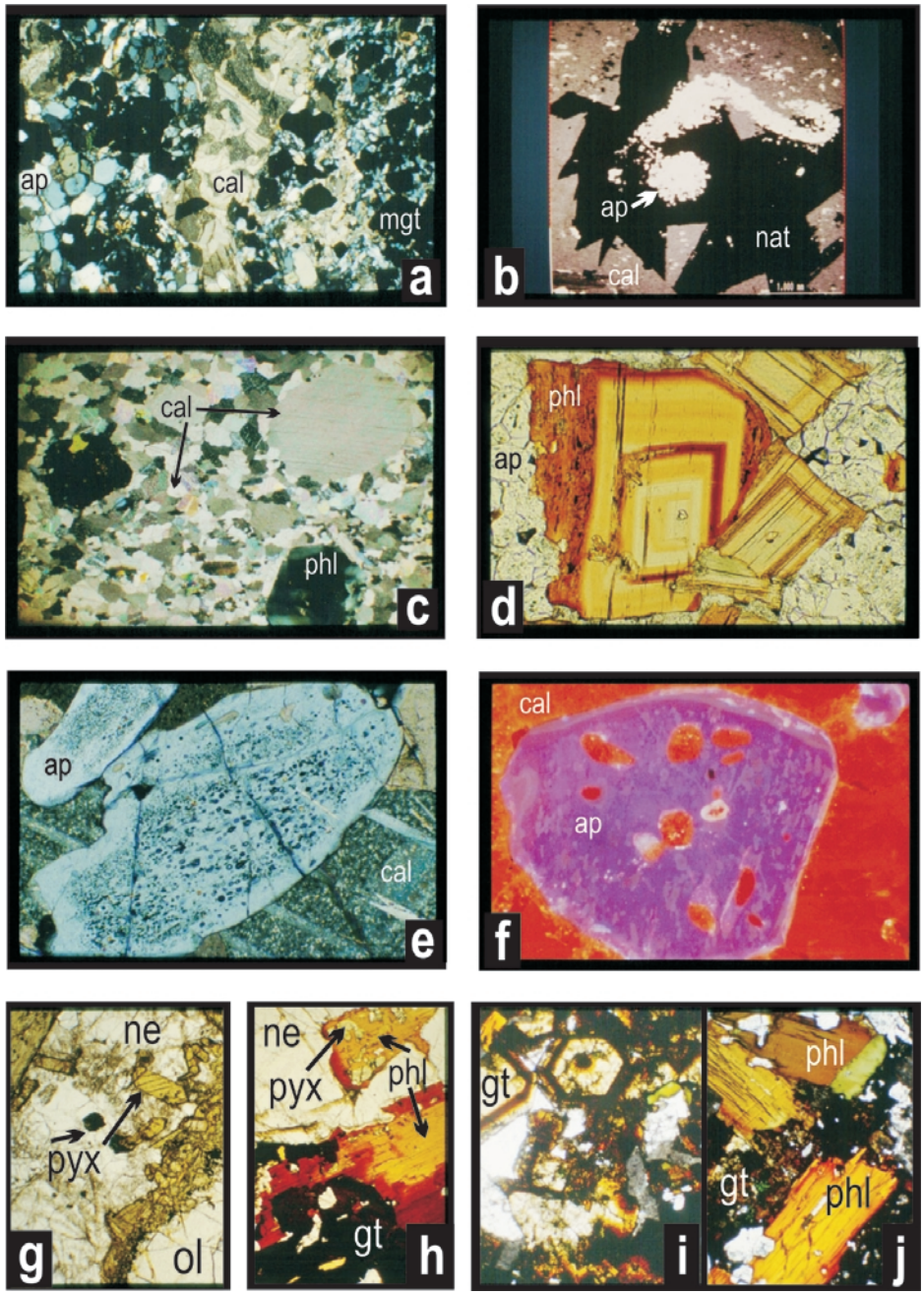

FIG. 2. (*a*) Carbonatite [C.6.15] exhibiting a coarse band of magnetite + apatite with interstitial calcite (left), a band of anhdedral calcite with interlocking grain boundaries (centre), and two bands of fine-grained apatite associated with relatively coarse magnetite, interspersed with calcite. Baddeleyite forms 10 μm-thick rims around the apatite crystals just to the left of the central calcite band. (*b*) Late-stage hydrothermal carbonatite [C.54.x], showing rhombohedral calcite (grey), natrolite (black) and an apatite vein (white). BSE image. (*c*) Carbonatite N.187.100 containing a round calcite phenocryst with strained extinction set in a finer-grained calcite groundmass. The

showing strained extinction, enclosed in a fine-grained, interlocking, calcite matrix (Fig. 2*c*).

The central-complex calcite carbonatites are more variable in mineralogy than the northern carbonatites. They contain tetra-ferriphlogopite showing reverse absorbtion and intense pleochroism (Fig. 2*d*) and/or richterite, with up to 30 modal % apatite, variable quantities of magnetite, and rare diopsidic pyroxene, but no melilite or garnet. The calcite-dolomite and dolomite carbonatites in the central complex represent the latest stages of carbonatite magmatism, and contain accessory apatite and sulphides but virtually no silicate minerals. Accessory minerals found in the carbonatites in this study include baddeleyite, baryte, calzirtite, chlorite (alteration), ilmenite (micro-intergrowth features in magnetite), quartz, perovskite, sulphides, titanite, zeolites, zircon and zirsinalite.

The greatest textural variations are exhibited by apatite and calcite. Apatite occurs as solitary, rounded grains, or as veins and/or clusters of tightly-packed grains, and also exhibits a variety of zoning patterns, textures and inclusions. Some apatite grains contain abundant small, tightly clustered, fluid-rich inclusions, while others contain elongate inclusions within their cores, paralleling the *c* crystallographic axis (Fig. 2*e*). In other samples, rounded apatite crystals occur at the junctions of calcite grains, typical of early carbonatites (Kapustin, 1980), and exhibit rare, large, solitary inclusions that contain carbonate or rare zircon as solid phases, in association with a fluid or vapour phase (Fig. 2*f*).

Four main textural styles of calcite crystals are recognized in the carbonatites. These are: (1) rounded crystals, fine- to coarse-grained, usually with strained extinction, found mainly in the early central complex carbonatites, and some of the northern melilite-bearing carbonatites. Some samples contain apatite crystals at calcite-crystal triple junctions. Similar features within the Kovdor carbonatites were assumed to be primary in origin (Zaitsev and Bell, 1995); (2) fine- to medium-grained, uniform extinction, and irregular interlocking grains, found most commonly in large volumes of pure calcite or where there are only small crystals of apatite located at the calcite grain corners; (3) large, rounded grains set in a fine-grained, interlocking calcite matrix characteristic of texture 2, as seen in Fig. 2*c*. Such grains probably represent phenocrysts or xenocrysts, which may have been partially resorbed within the enclosing melt. Similar textures have also been found in the Kontozero carbonatites (Ruklov, pers. comm., 2002). (4) medium- to coarse-grained, rhombohedral crystals with extensive concentric zoning. This feature has only been seen in the vein sample C.54.x (Fig. 2*b*).

Turjite

The southern coastal exposures on the Turiy Peninsula include turjite, the second type-locality rock found in this massif, believed to be part of the syn-massif or post-massif intrusion suites of dykes in this area (Bulakh and Ivanikov, 1984). Turjite, first defined by Beliankin and Kupletskii

hexagonal mineral at extinction is phlogopite. (*d*) Concentrically zoned phlogopite from carbonatite [C.49.40] alternating between tetra-ferriphlogopite (orange pleochroism, reverse absorbtion), and normal phlogopite (pale green–orange pleochroism, normal absorbtion). The groundmass consists mostly of fluid-inclusion-rich apatite. (*e*) Apatite crystals with inclusion-rich cores overgrown by inclusion-free rims. A few large, solitary inclusions can also be seen. (*f*) Cathodoluminscence image of apatite (purple) showing very mottled zonation throughout the crystal, surrounded by calcite crystals (orange) with rare interstitial blebs of dolomite (red). The apatite crystal contains a small train of fluid or calcite inclusions (left to right) and larger solitary inclusions, mostly filled with calcite and an unknown fluid phase. [Field of view = 2 mm (*a, c, d*); 0.5 mm (*e, f*). Cross-polarized light (*a, c*); Plane-polarized light (*d, e*)]. (*g*) Olivine melteigite sample C.AG.48A showing rounded, coarse-grained olivine with rims containing magnetite blebs (bottom right), and abundant augite including anhedral-euhedral grains <1−4 mm in diameter. Interstitial nepheline (centre) contains rare crystals of deep-green aegirine-augite. Mica is rare. (*h*) Urtite sample C.IJ.14 showing garnet (dark brown), tetra-ferriphlogopite (orange) enclosing and replacing clinopyroxene (green), all contained within abundant nepheline (pale grey). The pyroxene compositions match those of the groundmass compositions in the olivine melteigite. Significant quantities of primary pectolite also occur in this sample. (*i,j*) Turjite sample TU 119 showing euhedral and concentrically zoned andradite-melanite garnet (pale yellow–dark brown), anhedral areas of dark brown schorlomite, and grains of zoned phlogopite with variations in pleochroic colours dependent on crystal orientation. The groundmass contains anisotropic garnet and analcime. All photographs taken in plane polarized light. Fields of view ~1 mm. See text for details of the proposed relationship between the melteigite-urtite-turjite samples.

(1924), was later described by Le Maitre (1989) as a "melanocratic lamprophyre rich in biotite, analcime, calcite and melanite garnet". The reader is referred to Bell *et al.* (1996) for an extensive description of two type-locality samples [TU 119, TU120A].

Late-stage veins

The southern coastal exposures around the Turiy Peninsula contain a variety of late-stage veins, believed to have originated from fluids emanating from the main massif. These include veins of pectolite-wollastonite, calcite-quartz-fluorite-ankerite (sample TD 1) and aegirine-augite-apatite-ankerite (sample TD 2).

Analytical techniques

Most of the mineral analyses were obtained using a JEOL 733 electron microprobe at the Canadian Museum of Nature with 4 WDS spectrometers operating at 15 kV with a beam current of 20 nA and a beam diameter of ~10–30 μm. Data for microprobe standards were measured for 25 s or 0.25% precision per element, whichever was obtained first; data for the samples were measured for 25 s or to 0.5% precision, whichever was attained first. Cross-calibration checks were within analytical error. A selection of natural and synthetic standards was used. Data reduction was carried out using a ZAF correction program, and the FORMULA program was used to normalize the analyses. Mineral formulae were taken from Nickel and Nichols (1991). Mica analyses, where (Si+Al)<8 for 22 oxygen equivalents, were recalculated using the MICA program, whereby Fe^{2+} was converted to Fe^{3+} to fill the tetrahedral site, hence iteratively normalizing to 8 tetrahedral cations and 22 oxygen equivalents.

At Carleton University, a JEOL 3600 scanning electron microscope was used to obtain back-scattered-electron (BSE) photographs using a slide-maker with Ektachrome 100 slide film, and a Nikon microscope with Nuclide Luminescope® ELM Model 2B was used to obtain cathodoluminescence images of the massif samples. Samples were imaged at 12 kV, 0.2 millitorr and 0.5–0.6 mA.

Mg# is defined as $100[Mg/(Mg+Fe^{2+})]$ throughout this study, unless otherwise stated. Calculated Fe^{3+} (where applicable), is not included in the calculation of the Mg#.

Mineral compositions

Silicate minerals

Olivine and monticellite group minerals

Within the massif, olivine has only been found in the olivine melteigite pipe from the eastern side of the central complex (sample C.AG.48A). It has the composition Fo_{82-85}, and contains ~0.5 wt.% CaO and ~0.22–0.42 wt.% MnO. No significant core-to-rim compositional variations were seen.

Monticellite occurs in two melilite-bearing carbonatites from the northern complex. In one sample it is associated with diopside, vesuvianite and a variety of hydrous alkali-silicate minerals which have combined to replace melilite. In others, monticellite occurs as medium-grained crystals associated with garnet and phlogopite. Such mineral associations are typical of early carbonatites (Kapustin, 1980). The Mg# of the monticellite falls between 67.4 and 78.1, while MnO contents vary from 1.3 to 2.25 wt.%.

Garnet group

The garnet group is represented in Turiy by the $Ca_3(Fe^{3+},Ti^{4+},Al)_2(Si,Al,Fe^{3+})_3O_{12}$ solid solution (titangrandite) series with end-members andradite ($Ca_3Fe_2^{3+}Si_3O_{12}$), schorlomite ($Ca_3[Ti,Fe]_2[Si,Fe]_3O_{12}$) and grossular ($Ca_3Al_2Si_3O_{12}$). Some of the Si-rich melilitolite and turjite garnet analyses are believed to contain a small amount of the hibschite or katoite component ($Ca_3Al_2[(SiO_4),(OH)_4]_3$) causing anisotropy in the later garnet growth-stages. Garnet is one of the minerals that shows systematic variations in composition with rock type (Table 2), and is widespread in its occurrence and abundance throughout the massif.

Over the last 20 years there has been a great deal of work concerning the nature of cation substitutions in the tetrahedral site of minerals such as garnet (Locock *et al.*, 1995) and mica (Abrecht and Hewitt, 1988; Foley, 1989, 1990; Zhang *et al.*, 1993). While recognizing that co-ordination preferences depend on a number of factors including magma chemistry and oxygen fugacity, all garnet, mica and pyroxene analyses in this study were assumed to have $Si > Al > Fe^{3+}$ tetrahedral-site occupation preferences, while Ti^{4+}, Fe^{2+} and Mg were excluded from tetrahedral co-ordination. Garnet formulae were calculated with 16 cations:24 anions, realizing that the $Fe^{2+} \rightleftharpoons Fe^{3+}$ conversion enabled by this valence calculation makes no allowance for the varying valency of Ti or Mn, for any site vacancies, or for any hibschite component.

TABLE 2. Selected garnet compositions from a variety of rock types. All analyses normalized with 16 cations:24 anions.

Sample	C.90.29	C.AG.122		C.IJ.14	C.190.105	N.64.18	TUR I	C.54.x	N.64.19	TU 119	
Rock type	Pyroxenite	Ijolite		Urtite	Turjaite	Melilitolite	Turjaite	Carbonatite	Carbonatite	Turjite	
Analysis	PT 13	PT 12	PT 48	PT 7	PT 74	PT 44	PT 19	PT 73	PT 63	PT 70	PT 76
SiO_2	33.17	33.66	27.00	30.05	33.94	35.96	37.19	35.14	36.34	34.76	28.72
TiO_2	6.33	5.06	16.72	12.11	5.05	1.24	0.28	1.70		2.30	15.29
Al_2O_3	1.00	0.92	1.88	0.84	3.76	3.23	6.38	1.41	3.91	0.55	0.50
Fe_2O_3	23.86	25.96	16.68	20.00	22.24	25.03	21.53	27.01	25.22	27.99	15.13
FeO	2.04	0.27	3.43	3.32	0.67		0.55	0.40		0.51	2.79
MnO	0.33	0.22	0.28	0.26	0.17		0.10	0.13	0.10	0.36	0.43
MgO	0.39	0.40	1.11	0.80	0.65	0.25	0.18	0.39	0.18	0.14	1.05
CaO	32.46	33.63	31.91	32.02	33.66	34.09	34.15	33.03	33.82	32.67	30.99
Na_2O	0.15	0.11	0.16	0.17						0.14	0.71
Total	99.73	100.23	99.17	99.57	100.14	99.80	100.36	99.22	99.57	99.42	95.61
Si	5.604	5.649	4.615	5.113	5.619	5.967	6.040	5.929	6.030	5.890	5.048
^{iv}Al	0.199	0.182	0.379	0.168	0.381	0.033		0.071		0.110	0.104
$^{iv}Fe^{3+}$	0.197	0.169	1.006	0.719						0.000	0.848
^{vi}Al					0.353	0.599	2.631	0.209	0.765		
$^{vi}Fe^{3+}$	2.836	3.110	1.139	1.842	2.771	3.125	1.221	3.430	3.149	3.569	1.153
Ti	0.804	0.639	2.149	1.550	0.629	0.155	0.034	0.216		0.293	2.021
Fe^{2+}	0.289	0.038	0.491	0.473	0.093		0.074	0.057		0.073	0.410
Mn	0.047	0.031	0.041	0.037	0.024		0.014	0.019	0.014	0.052	0.064
Mg	0.098	0.100	0.283	0.203	0.160	0.062	0.044	0.098	0.045	0.035	0.275
Ca	5.876	6.047	5.844	5.838	5.971	6.060	5.942	5.971	6.012	5.932	5.836
Na	0.049	0.036	0.053	0.056						0.046	0.242
Total	16.000	16.001	16.000	16.000	16.000	16.000	16.000	16.000	16.014	16.000	16.001

Blank spaces: below detection limit

In all garnet analyses from the rock types investigated from Turiy, Ca never falls below 96.5% occupancy of the distorted cubic A site. Sr is found in some samples.

Following the site-occupancy guidelines outlined above, the incorporation of Ti^{4+} into the *M* site causes the need for coupled substitutions such as:

$$^{iv}Si^{4+} + {}^{vi}(Al^{3+},Fe^{3+}) \rightleftharpoons {}^{iv}(Al^{3+},Fe^{3+}) + {}^{vi}Ti^{4+} \quad (1)$$

$$^{vi}[(Mg,Fe^{2+}) + Ti^{4+} \rightleftharpoons (Al,Fe^{3+})_2] \quad (2)$$

In the Turiy rocks, garnet rich in Ti appears to follow scheme 1 until it reaches Ti = ½ octahedral-site occupancy (schorlormite, ~15 wt.% TiO_2), after which substitution is dominated by scheme 2.

Garnet is most abundant in the ijolite–urtite series rocks, where garnet and phlogopite increase in abundance relative to pyroxene as the abundance of nepheline increases. Garnet in these rocks is rich in the schorlomite component, with concentric zonation between andradite (pale green) and schorlomite (dark brown). The melilite-bearing rocks contain rare Al-rich andradite which is probably formed as a late-stage reaction product between melilite and residual magmatic fluids, or by melilite break-down. In these rocks, garnet normally forms veins and rims along grain-boundaries. Only in 'pegmatitic' melilitolites (e.g. sample TUR I), does garnet form fine- to medium-grained brown anhedral crystals, relatively rich in Ti, which may grade into colourless veins of anisotropic andradite around melilite, or magnetite and perovskite (Bell *et al.*, 1996). The anisotropy is probably caused by a small amount of the hibschite component.

The data plotted in Fig. 3 show a clear distinction between garnet compositions from the ijolite and melilitolite series. All garnet analyses from the melilitolites have (Si+Al) > 6 cations, with the excess Al creating ^{vi}Al and thus a presumed absence of $^{iv}Fe^{3+}$ along with low Ti content. Conversely, garnets from the ijolite series typically have (Si+Al) < 6 cations, leading to rare ^{vi}Al but persistent calculated $^{iv}Fe^{3+}$, along with increasing Ti content. It is important to note that the Si content of the melilitolite garnets is substantially greater than that of the ijolite garnets, and thus Fig. 3 should not be interpreted in terms of Al abundance, but rather Al (and Fe^{3+}) site allocation and cation co-ordination. The overall range in composition of the turjite garnet analyses encompasses most of the melilitolite and ijolite garnet compositions, thus emphasizing the hybrid nature of this unusual rock-type. The carbonatite ^{vi}Al-bearing analyses are from garnet from the northern carbonatites associated with melilitolites, and some of these carbonatites also contain melilite. Those carbonatite garnet analyses which fall on the $^{iv}Fe^{3+}$ side of the *x* axis in Fig. 3 were obtained from sample N.63.4., a pyroxene-calcite rock from the northern massif.

Melilite group

Melilite occurs most commonly in Si-poor, Ca-rich environments, and is an important mineral at Turiy. Its principal solid-solution components are $Ca_2(Mg,Fe^{2+})Si_2O_7$ ($akermanite_{ss}$), $CaNaAlSi_2O_7$ (soda-melilite) and $Ca_2Al_2SiO_7$ (gehlenite) (Deer *et al.*, 1986).

Significant variations in melilite composition occur in the Turiy samples (Table 3). The high soda-melilite content (Na=Al=1 = 50% soda-melilite component) correlates with the high abundances of volatile and alkali-rich minerals in the silicate samples. Melilite from the two melilite-calcite carbonatite samples [N.64.18m, N.64.19] from the northern complex contains a distinct and much lower soda-melilite component (~30%), quite separate from the melilite compositions in the silicate rocks. The presence of the gehlenite component in melilite from the ultra-melilitolite sample TUR II may be linked to the cumulate nature of this sample.

The Mg#s of melilite show an approximate inverse correlation to Na content, with the array

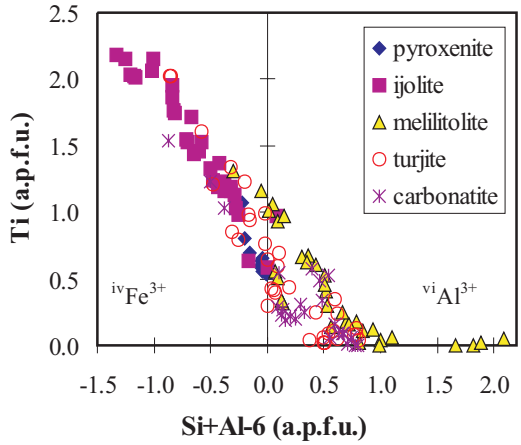

FIG. 3. Garnet compositions from the Turiy rocks. All analyses normalized with 16 cations:24 anions, assuming Si > Al > Fe^{3+} occupancy preference within the 6-cation tetrahedral site. See text for further explanation.

TABLE 3. Selected melilite compositions from a variety of rock types. All analyses normalized with 10 cations:14 anions.

Sample	C.5.118	C.190.105	N.64.19	N.64.18	E.133.30	TUR II	TUR I
Rock type	Phlog. turj.	Turjaite	Mel. carb.	Calc. mel.	Turjaite	Ultramel.	Phlog. turj.
Analysis	PT 2	PT 66	PT 66	PT 42	PT 53	PT 15	PT 11
SiO_2	43.73	44.05	43.51	43.64	43.02	44.09	45.11
Al_2O_3	8.43	9.45	6.02	5.59	7.17	7.74	9.08
Fe_2O_3	1.54	0.33	1.39	1.57	0.68		0.20
FeO	2.20	2.41	1.58	0.92	3.32	2.30	2.36
MnO	0.09	0.09	0.17	0.19	0.13		0.07
MgO	6.05	6.29	8.60	9.04	6.31	7.83	6.36
SrO	0.63	0.64	0.47	0.34	0.97		0.95
CaO	32.13	31.21	34.28	35.27	32.54	34.24	30.32
K_2O					0.04		
Na_2O	5.19	5.42	3.67	3.44	4.34	3.95	5.92
Total	100.00	99.89	99.70	100.01	98.53	100.15	100.37
Si	3.953	3.960	3.953	3.950	3.977	3.957	4.028
Al	0.898	1.001	0.645	0.596	0.781	0.819	0.956
Fe^{3+}	0.105	0.023	0.095	0.107	0.048		0.013
Fe^{2+}	0.167	0.181	0.120	0.070	0.257	0.173	0.176
Mn	0.007	0.007	0.013	0.015	0.010		0.005
Mg	0.815	0.843	1.165	1.220	0.870	1.048	0.847
Sr	0.033	0.033	0.025	0.018	0.052		0.049
Ca	3.112	3.006	3.337	3.420	3.223	3.293	2.901
K					0.005		
Na	0.910	0.945	0.647	0.604	0.778	0.688	1.025
Total	10.000	10.000	10.000	10.000	10.000	9.978	10.000

Rock-type abbreviations: Turj = turjaite; Mel. carb. = melilite carbonatite; Calc. mel. = calcite melilitolite; Ultramel. = ultramelilitolite
Blank spaces: below detection limit

shown in Fig. 4*b* probably reflecting an overall fractionation trend with increasing Na-Fe content. The melilite compositions from sample TUR I, which lie above the trend, reflect the alkali-enriched nature of the sample by lying on the Na-rich side of the Na-Mg# trend defined by compositions from the other silicate samples. The analyses from the two melilite-calcite-carbonatites again fall in a Mg-rich cluster quite separate from the melilite compositions from silicate rocks.

Pyroxene group

Pyroxene compositions range from pure diopside to 80 mol.% aegirine, and also encompass aluminian sub-silicic augites, that contain calculated tschermakitic components such as $CaTiAl_2O_6$, $CaFe^{3+}AlSiO_6$, $CaAl_2SiO_6$, $CaFe^{3+}_2SiO_6$ and $Na[Ti_{0.5}(Fe^{2+},Mg)_{0.5}]Si_2O_6$ (Table 4). Like garnet, the pyroxene compositions can relate to the rock type in which they occur, although the systematic compositional variations are generally less distinct. All clinopyroxene analyses have been normalized on the basis of 4 cations:6 anions valence calculation, and Mg# = $Mg/(Mg+Fe^{2+})$.

Table 4 includes three major variants in pyroxene compositions: Mg#, aegirine content, and the calculated Tschermak component content for the selected compositions shown. The aegirine *vs*. Tschermak component contents are plotted in Fig. 5. Although there is distinct overlap in pyroxene compositions among the different rock-types, some significant correlations and groupings can be seen. Compositions from the pyroxenites, a calcite-pyroxene rock [N.63.4] and melilitolite sample TUR I are rich in Tschermak-components. Most of the central massif carbona-

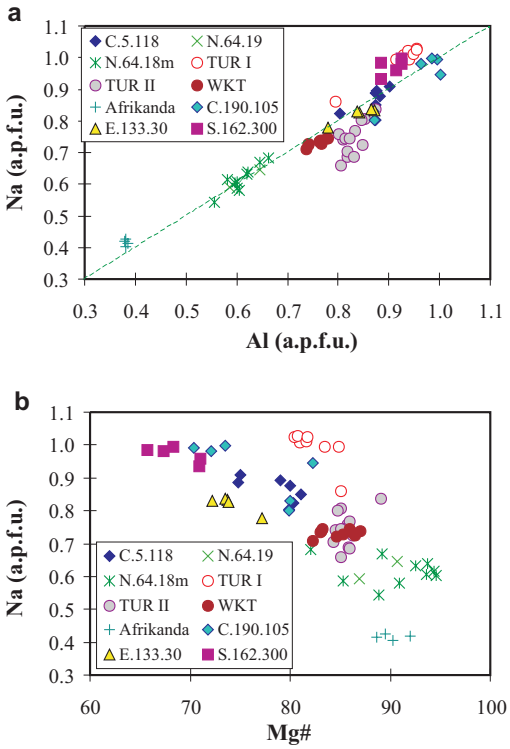

FIG. 4. Melilite compositions from the Turiy rocks. (*a*) Na-Al plot demonstrating the amount of the soda-melilite component (Na = Al = 1 = 50% [$CaNaAlSi_2O_7$]), the presence of the gehlenite component [$Ca_2Al_2SiO_7$] (Al > Na) and the $CaNaFe^{3+}Si_2O_7$ component (Na > Al). Analyses from the northern complex melilite carbonatite and calcite melilitolite samples [N.64.18m and N.64.19] contain smaller quantities of the soda-melilite component than the analyses from the silicate rocks (all other analyses). 'Afrikanda' = analyses from a melilite-bearing olivinite from the Afrikanda massif. (*b*) Na-Mg# plot demonstrating the fractionation trend between the akermanite and soda-melilite components. The analyses from the melilite-calcite samples from the northern complex [N.64.18m and N.64.19] have the highest Mg#s.

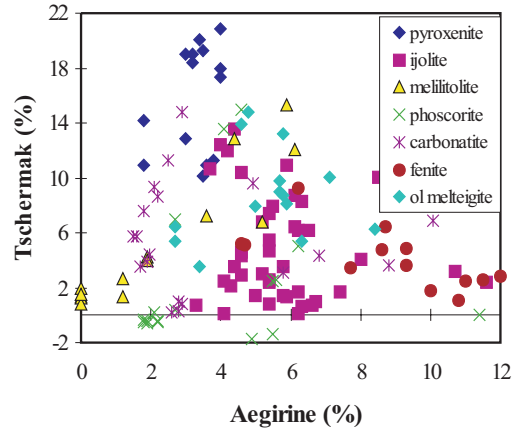

FIG. 5. Clinopyroxene compositions from the Turiy rocks plotting mol.% aegirine *vs*. mol.% Tschermak components ($CaAl_2SiO_6$, $CaFe^{3+}AlSiO_6$, $CaFe^{3+}_2O_6$ and $CaTiAl_2O_6$). Up to 80% of the aegirine component is found in the fenite pyroxenes (off-scale).

tites and phoscorite sample C.K.7 have pyroxene compositions with very high Mg#s and very low aegirine and Tschermak components. Pyroxene with high aegirine content, and minimal Tschermak content is found in a few of the ijolites, the late-stage groundmass pyroxenes in the olivine melteigite [C.AG.48A], the late-stage aegirine-apatite-ankerite vein TD 2, and the fenites. Mg#s are also low in all of these samples. Samples with intermediate values of all three variables generally belong to the ijolite series. In addition, the small quantities of the unusual component [$Na(Ti_{0.5},Mg_{0.5})Si_2O_6$] are needed to charge-balance the phoscorite and late-stage olivine melteigite pyroxene compositions, as well as analyses from a hybrid melilitolite-ijolite sample, S.162.300.

The pyroxenoid wollastonite is found in trace quantities in the melilite-calcite samples N.64.19 and N.64.18m, and as coarse anhedral grains in the melilitolite-ijolite contact sample S.162.300.

The existence of two ijolite series, based on field studies (e.g. Bulakh and Ivanikov, 1984), is not reflected by the chemical composition of the pyroxenes, nor by their mafic indices.

Amphibole group

Amphiboles are not common at Turiy, and are absent entirely from the ijolite and melilitolite series. Magnesio-hastingsite (*sensu* Leake, 1978) occurs as an intercumulus phase in the pyroxenites. Richterite is found in the phoscorites and carbonatites, and occurs as radiating clusters of elongate crystals, which are probably either late-stage or secondary in most samples. Rare magnesio-arfvedsonite has been found in two samples, while ferroan pargasitic hornblende (*sensu* Leake, 1978) was found within the fenite sample NC.153.82. The reason for the low abundance of amphibole in the Turiy rocks, and its complete absence from the melilitolites and ijolites, where mica is the dominant volatile-rich

TABLE 4. Selected pyroxene compositions from a variety of rock types. All analyses normalized with 4 cations:6 anions.

Sample	C.AG.347	C.AG.48A			C.AG.122	C.IJ.14	E.123.106		E.133.30	TUR I	C.K.7	C.TL.344	N.63.4	N.64.19	TD 2	NC.153.82
Rock type	Pyxite	Ol. melteigite			Ijolite	Ijolite	Ijolite		Turjaite	Turjaite	Phosc.	Carb.	Carb.	Carb.	Aeg.-ap. vein	Fenite
Analysis	PT 63	PT 28	PT 58	PT 55	PT 1	PT 16	PT 3	PT 5	PT 41	PT 2	PT 42	PT 66	PT 64	PT 58	PT 34	PT 63
SiO_2	46.47	49.78	52.53	51.26	50.32	51.20	49.76	51.78	53.80	49.34	54.67	54.55	51.12	53.06	52.21	53.02
TiO_2	2.81	1.63	0.85	0.28	0.88	1.15	0.36	0.68		0.75	0.49	0.31	0.81	0.25	0.18	0.54
Al_2O_3	6.22	3.46	1.14	0.76	3.00	2.04	0.61	1.19	0.88	4.29	0.18	0.37	2.52	1.33	0.56	0.35
Fe_2O_3	4.92	4.28	1.93	10.11	4.24	3.58	12.24	2.83		6.35	0.74	0.52	3.05	1.67	15.77	10.51
FeO	1.79	2.96	2.34	10.91	3.09	4.24	13.43	4.76	5.31	1.73	3.86	2.51	2.01	2.09	3.08	5.83
MnO	0.09	0.10	0.08	0.59	0.20	0.20	0.71	0.32	0.23	0.19	0.17	0.12	0.31	0.26	0.82	0.30
MgO	13.05	13.16	15.62	4.88	13.40	13.32	2.24	13.20	14.68	12.92	15.81	16.44	14.73	15.71	6.74	8.46
SrO	0.16	0.13	0.24	0.16	0.10	0.15	0.20	0.13	0.09		0.09		0.15	0.19		0.13
CaO	24.11	23.25	24.17	15.64	24.43	23.47	14.73	24.12	24.74	24.13	23.39	24.86	24.77	24.96	13.59	15.97
Na_2O	0.42	0.99	0.47	4.57	0.52	0.84	4.89	0.63	0.17	0.82	0.77	0.37	0.31	0.26	6.31	4.77
Total	100.04	99.74	99.37	99.16	100.18	100.19	99.17	99.64	99.90	100.53	100.16	100.05	99.78	99.78	99.26	99.88
Si	1.731	1.854	1.942	1.999	1.869	1.903	1.980	1.938	1.988	1.826	2.000	1.990	1.891	1.950	1.989	2.002
Al^{iv}	0.269	0.146	0.050	0.001	0.131	0.089	0.020	0.052	0.012	0.174		0.010	0.109	0.050	0.011	
Fe^{3+iv}			0.008			0.008		0.010								
Al^{vi}	0.004	0.006		0.034			0.009		0.026	0.014	0.008	0.006	0.001	0.008	0.014	0.016
Fe^{3+vi}	0.138	0.120	0.046	0.297	0.119	0.092	0.367	0.070		0.177	0.020	0.014	0.085	0.046	0.452	0.299
Ti	0.079	0.046	0.024	0.008	0.025	0.032	0.011	0.019		0.021	0.013	0.009	0.023	0.007	0.005	0.015
Fe^{2+}	0.056	0.092	0.072	0.356	0.096	0.132	0.447	0.149	0.164	0.054	0.118	0.077	0.062	0.064	0.098	0.184
Mn	0.003	0.003	0.003	0.019	0.006	0.006	0.024	0.010	0.007	0.006	0.005	0.004	0.010	0.008	0.026	0.010
Mg	0.725	0.731	0.861	0.284	0.742	0.738	0.133	0.736	0.809	0.713	0.862	0.894	0.812	0.861	0.383	0.476
Sr	0.003	0.003	0.005	0.004	0.002	0.003	0.005	0.003	0.002		0.002	0.000	0.003	0.004		0.003
Ca	0.962	0.928	0.957	0.653	0.972	0.935	0.628	0.967	0.979	0.957	0.917	0.971	0.982	0.983	0.555	0.646
Na	0.030	0.071	0.034	0.345	0.037	0.061	0.377	0.046	0.012	0.059	0.055	0.026	0.022	0.019	0.466	0.349
Total	4.000	4.000	4.000	4.000	4.000	4.000	4.000	4.000	3.999	4.001	4.000	4.000	4.000	4.000	4.000	4.000
Mg#	92.8	88.8	92.3	44.4	88.5	84.8	22.9	83.2	83.1	93.0	88.0	92.1	92.9	93.1	79.6	72.1
Aeg.%	3.0	7.1	3.4	34.5	3.7	6.1	37.7	4.6	1.2	5.9	5.5	2.6	2.2	1.9	46.6	34.9
Tsch.%	19.1	10.0	3.5	-0.7	10.7	6.4	1.0	4.3	1.3	15.3	-1.4	0.2	8.7	4.3	0.6	−1.7

Aeg.% = mol.% aegirine; Tsch.% = mol.% Tschermak components ($CaTiAl_2O_6$, $CaFe^{3+}AlSiO_6$, $CaAl_2SiO_6$, Ca $Fe_2^{3+}SiO_6$); Mg# = (100*Mg/(Mg+Fe^{2+}))
Rock-type abbreviations: Pyxite: pyroxenite; Phosc.: phoscorite; Carb.: carbonatite; Aeg.-ap.: aegirine-apatite
Blank spaces: below detection limits

TABLE 5. Selected mica compositions from a variety of rock types. All analyses normalized with 8 tetrahedral cations and 22 anions.

Sample	C.AG.48A	C.AG.122	C.5.118		E.133.30	TUR I	C.K.7	C.3.93	C.19.163	
Rock type	Ol. melt.	Ijolite	Turjaite		Turjaite	Turjaite	Phosc.	Phosc.	Phosc.	
Analysis	PT 73	PT 50	PT 26	PT 27	PT 39	PT 23	PT 53	PT 4	PT 20	PT 21
SiO_2	40.38	40.62	39.11	35.70	38.36	36.54	41.86	41.67	41.79	42.11
TiO_2	0.65	0.55	1.43	3.69	1.67	2.67	0.28	0.19	0.34	0.14
Al_2O_3	12.39	12.10	13.47	15.46	14.16	15.66	9.84	5.29	11.37	6.90
Fe_2O_3	0.33	0.26					3.41	8.93	1.08	6.61
FeO	9.39	8.61	9.25	9.74	9.62	7.45	3.37	4.71	3.62	3.13
MnO	0.15	0.25	0.22	0.18	0.19	0.08	0.10	0.09		
MgO	22.09	22.26	20.97	18.83	20.63	21.28	25.99	24.33	25.77	25.71
CaO	0.08	0.07	0.09		0.10	0.05	0.07	0.10	0.24	0.09
BaO	0.49	0.60	0.43	1.71	0.82	1.42				
Na_2O	1.27	0.30	0.26	0.27	0.37	0.61	0.90	0.38	0.20	0.26
K_2O	8.55	10.21	10.19	9.61	9.93	9.17	9.54	10.03	10.52	10.14
H_2O	3.08	2.81	4.12	3.68	3.68	3.73	4.20	3.68	4.23	4.13
F	2.16	2.69		0.76	0.88	0.75		0.87		
Cl										
O=F+Cl	−0.91	−1.13		−0.32	−0.37	−0.32		−0.37		
Total	100.07	100.18	99.54	99.31	100.04	99.09	99.56	99.90	99.16	99.22
Si	5.849	5.900	5.721	5.317	5.613	5.364	5.978	6.103	5.970	6.101
^{iv}Al	2.115	2.071	2.279	2.683	2.387	2.636	1.656	0.913	1.914	1.178
$^{iv}Fe^{3+}$	0.036	0.029					0.366	0.984	0.116	0.721
^{vi}Al			0.044	0.031	0.055	0.074				
Ti	0.071	0.060	0.157	0.413	0.184	0.295	0.030	0.021	0.037	0.015
Fe^{2+}	1.138	1.046	1.132	1.213	1.177	0.915	0.402	0.577	0.432	0.379
Mn	0.018	0.031	0.027	0.023	0.024	0.010	0.012	0.011		
Mg	4.770	4.820	4.573	4.181	4.500	4.657	5.533	5.312	5.488	5.553
Ca	0.012	0.011	0.014		0.016	0.008	0.011	0.016	0.037	0.014
Ba	0.028	0.034	0.025	0.100	0.047	0.082				
Na	0.357	0.084	0.074	0.078	0.105	0.174	0.249	0.108	0.055	0.073
K	1.580	1.892	1.902	1.826	1.854	1.717	1.738	1.874	1.917	1.874
Total	15.974	15.978	15.947	15.865	15.961	15.932	15.975	15.919	15.966	15.908

silicate phase, is not entirely clear. Hogarth (1989) lists amphibole as one of the commonest minerals in carbonatites, yet its presence in the Turiy samples is always <5 modal % in the few carbonatites in which it occurs.

Mica group

Phlogopite [$K_2Mg_6Al_2Si_6O_{20}(OH,F,Cl)_4$], exhibiting extensive solid solution, is present in all rock types in Turiy except the pyroxenites (Table 5). Different rock-types are characterized by specific mica compositions, in a similar way to the garnet and pyroxene groups. The possiblity of using micas as 'indicator minerals' in such massifs was noted by Kapustin (1980).

Interlayer site substitutions are minimal in most samples and include minor amounts of Ba (common in phlogopite from alkalic rocks, e.g. Zhang, 1993; Henderson and Foland, 1996) and trace amounts of Na and Ca. The octahedral cation site, filled primarily by Mg, also contains Fe, Mn, Al and Ti in the Turiy micas. Such substitutions in both sites exhibit a maximum in the melilitolites, and a minimum in the phoscorites.

In the normalization procedures used for micas in this study it was assumed that the tetrahedral site would maintain full occupancy, and the number of anions would also be a maximum. Similar assumptions were made by Hogarth (1997). The first of these assumptions is probably correct, but the second fails to take into account the possible substitution of OH^- for O^{2-} (Zhang, 1993), although it is difficult to identify samples in which this substitution mechanism occurs.

TABLE 5 (*contd.*)

Analysis	C.6.15 Carb. PT 11	C.6.15 Carb. PT 19	C.49.40 Carb. PT 53	C.49.40 Carb. PT 54	C.100.d Carb. PT 20	N.64.19 Carb. PT 61	TU 119 Turjite PT 25	TU 120A Turjite PT 5
SiO_2	42.49	40.16	42.92	42.40	42.43	40.27	39.02	38.40
TiO_2	0.11	1.02	0.35	0.22	0.08	0.22	1.26	1.50
Al_2O_3	9.01	12.14	10.68	2.74	11.56	13.92	10.63	12.77
Fe_2O_3	4.45	0.70	1.86	11.80	0.93		1.24	
FeO	1.34	9.62	2.89	4.16	2.12	5.58	17.35	12.09
MnO		0.19		0.06		0.21	0.57	0.55
MgO	27.41	21.41	26.42	24.58	27.30	24.76	15.13	18.82
CaO	0.10		0.15	0.26			0.22	
BaO		0.17	0.30		0.18	0.30	0.13	0.66
Na_2O	0.43	0.71	0.26	0.28	0.25	0.78	0.19	
K_2O	10.44	9.81	10.69	9.23	10.70	9.64	9.69	10.15
H_2O	3.94	3.90	3.79	4.03	3.96	4.20	3.93	4.01
F	0.51	0.45	0.89		0.59			
Cl								
O=F+Cl	−0.21	−0.19	−0.37		−0.25			
Total	100.02	100.09	100.83	99.76	99.85	99.88	99.36	98.95
Si	6.021	5.842	6.033	6.223	5.981	5.743	5.948	5.747
^{iv}Al	1.505	2.081	1.769	0.474	1.921	2.257	1.910	2.252
$^{iv}Fe^{3+}$	0.475	0.077	0.197	1.303	0.098		0.142	
^{vi}Al						0.083		
Ti	0.012	0.112	0.037	0.024	0.008	0.024	0.144	0.169
Fe^{2+}	0.159	1.170	0.340	0.511	0.250	0.666	2.212	1.513
Mn		0.023		0.007		0.025	0.074	0.070
Mg	5.790	4.643	5.537	5.378	5.737	5.264	3.438	4.199
Ca	0.015		0.023	0.041			0.036	
Ba		0.010	0.017		0.010	0.017	0.008	0.039
Na	0.118	0.200	0.071	0.080	0.068	0.216	0.056	
K	1.887	1.820	1.917	1.728	1.924	1.754	1.884	1.938
Total	15.982	15.978	15.941	15.769	15.997	16.049	15.852	15.927

Rock-type abbreviations: Phosc. = phoscorite; Carb. = carbonatite; melt. = melteigite
Blank spaces: below detection limit

Iterative normalization based on 8 tetrahedral cations and 22 oxygen-equivalents allows for conversion of $^{vi}Fe^{2+}$ to $^{iv}Fe^{3+}$ to fill vacancies in the tetrahedral site while maintaining charge-balance, and still allows for vacancies in the octahedral and inter-layer sites. Any remaining Fe is assumed to be $^{vi}Fe^{2+}$. A similar normalization scheme was devised by Araújo (1996) and also used successfully for rocks similar to those found at Turiy by Brod *et al.* (2001). The presence of $^{iv}Fe^{3+}$ substituting for ^{iv}Al is marked by orange pleochroism and reverse absorption (Rimsakaya-Korsakova and Sokolova, 1964; Kapustin, 1980; Gaspar and Wyllie, 1987), which is seen in micas from the phoscorites, carbonatites, turjite and some ijolites from Turiy, and correlates well with the results of the iterative normalization procedure.

The melilitolite micas, rich in ^{vi}Al, invariably exhibit brown-straw colour pleochroism while ^{vi}Al-bearing micas from the northern carbonatites exhibit pale, green-straw pleochroism, typical of micas from early carbonatites, (Kapustin, 1980). The phoscorite and central-complex carbonatite micas, rich in $^{iv}Fe^{3+}$, show bright orange–pale orange pleochroism and reverse absorption, leading to $^{iv}[Al_{0.5}Fe^{3+}_{1.5}Si_6]$ tetra-ferriphlogopite compositions in the most extreme case [carbonatite sample C.49.40]. Micas from turjite sample TU 120A show both pale green/brown and orange pleochroism, correlated with the change from calculated ^{vi}Al to $^{iv}Fe^{3+}$-bearing compositions and

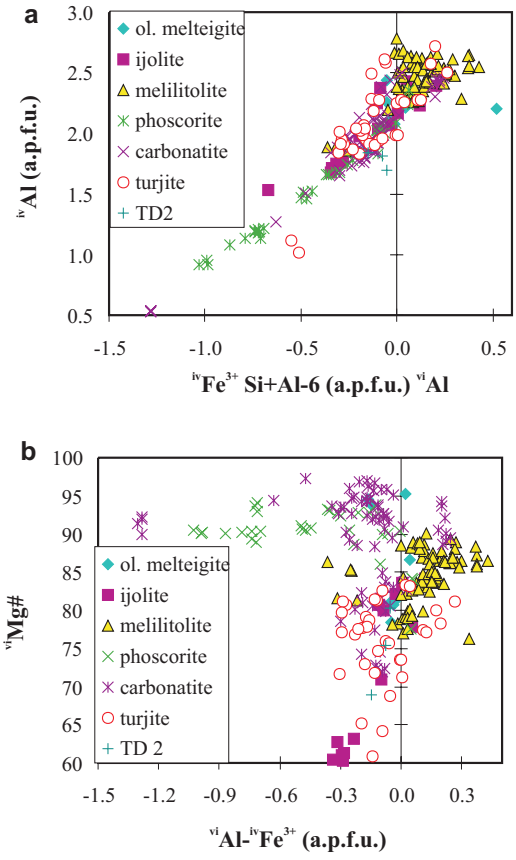

FIG. 6. (*a*) Mica compositions from the Turiy rocks plotting ^{vi}Al, ^{iv}Al and ^{iv}Fe^{3+} contents. Any analyses with ^{iv}Al >2 imply that Al is also substituting for Si. TD 2 = a late-stage aegirine-augite-apatite-ankerite vein on the south coast. (*b*) Mica compositions from the Turiy rocks demonstrating the relationship between octahedral site Mg# and ^{vi}Al-^{iv}Fe^{3+} occurrence. See text for further explanation.

a corresponding change from normal to reverse absorption. The correlation between pleochroic scheme, absorption and composition outlined above is best indicated in a plot of ^{iv}Al *vs.* ^{vi}Al-^{iv}Fe^{3+} (Fig. 6*a*). Micas from melilite-bearing silicate and carbonatite samples contain ^{vi}Al and have the highest total Al content. Other ^{vi}Al-bearing mica analyses come from a phoscoritized pyroxenite, and three ijolite samples located spatially close to melilitolites within the massif. Those turjite mica analyses which plot in the ^{vi}Al-bearing area are from a sample with relict melilite from the chilled margin of a dyke. With few exceptions, a clear distinction can be drawn between the melilite-bearing and the non-melilite-bearing samples on the basis of Al contents and site allocations within the micas, even though there are no distinct compositional breaks between the rock-types.

A plot of mica ^{vi}Mg# *vs.* ^{vi}Al-^{iv}Fe^{3+} (Fig. 6*b*) shows distinct groupings and different fractionation trends. A trend shown by the carbonatites and phoscorites exhibits consistently high ^{vi}Mg#s with changing ^{iv}Fe^{3+} contents, while a second trend shown by most analyses from the silicate rocks exhibits decreasing Mg# with increasing ^{iv}Fe^{3+} content. Such trends are typical of micas from these types of rocks (Brod *et al.*, 2001). A cluster of melilitolite-ijolite-carbonatite-turjite mica analyses lies between these two trends, with Mg# values of ~80. The cluster of carbonatite mica analyses around (0.25, 93) in Fig. 6*b* are from a late-stage natrolite-calcite carbonatite vein (Fig. 2*b*).

Feldspathoid group

Nepheline is an essential phase in the ijolites and most melilitolites from Turiy, and a minor constituent of the pyroxenites. It is not found in the carbonatites, phoscorites or fenites, although Bulakh and Ivanikov (1996) report trace quantities of nepheline in some late-stage carbonatites. No separate potassic feldspathoids such as leucite and kalsilite have been found at Turiy.

All nepheline compositions fall between 70 and 90% $NaAlSiO_4$. There is no systematic variation between the compositions of nepheline from the ijolite and melilitolite series rocks, although average compositions indicate that the melilitolite nephelines are slightly more enriched in the $NaAlSiO_4$ component. The nepheline from the groundmass of the olivine melteigite [C.AG.48A] is the most enriched in the $NaAlSiO_4$ component (90%).

Feldspar group

Feldspars are very limited in occurrence within any of the rocks from the Turiy complex. Sample TD 2 is the closest approximation to a feldspar-bearing 'carbonatite', containing 20% [ankerite + calcite] and almost pure albite and K-feldspar, in the groundmass. The fenite sample [NC.153.82] contains abundant feldspar, most of which is either pure albite or K-feldspar with 3–45% albite exsolution. Coarse-grained, rounded crystals of K-feldspar in sample NC.153.82 also contain wollastonite within apparent perthitic

exsolution lamellae. Euhedral celsian [$BaAl_2Si_2O_8$] is a significant component of the groundmass of turjite sample TU 120A.

Tektosilicates

In a silica-depleted intrusion such as Turiy, quartz is rare, but occurs interstitially within the groundmass in the calcite-fluorite vein sample TD 1, where it encloses rare Nb-rich anatase/brookite(?) needles.

Hydrous alkali-silicates are common as groundmass minerals in some samples. Analcime is the main constituent of the groundmass in turjite sample TU 119 and is also found in the fenitized country rock sample NC.153.82. Natrolite is an abundant component in carbonatite sample C.54.x where it surrounds veins of apatite and concentrically zoned, rhombohedral calcite (Fig. 2*b*), typical of natrolite occurrences in late carbonatite veins (Kapustin, 1980). Natrolite is also found in both ijolite-fenite contact samples. Cuspidine, which occurs in the melilitolites in trace quantities, contains up to 14 wt.% F.

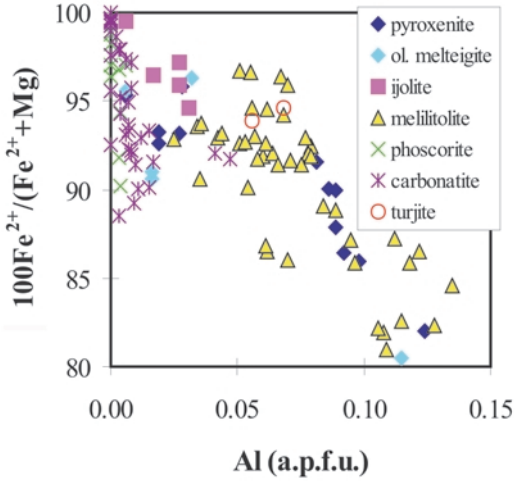

FIG. 7. Magnetite compositions from the Turiy rocks. Note that the melilitolite, pyroxenite and turjite magnetite analyses have higher Al contents than the rest of the samples. Most of the olivine melteigite data is off scale, due to the presence of a significant spinel component in the analyses. $Fe^{2+}\# = 100(Fe^{2+}/(Fe^{2+}+Mg))$.

Non-silicates

Fe-(Ti) oxides

Members of both the titanian magnetite (spinel) and ilmenite series are present at Turiy. Ilmenite almost invariably occurs as micro-intergrowths within magnetite, rich in Mg or Mn. Such intergrowths can take a number of forms (Lattard, 1995), and the typical lamellae described by Buddington and Lindsley (1964) are rare in Turiy magnetites. Instead, irregular, almost interstitial ilmenite blebs, rarely more than 20 μm in diameter, are far more common. However, they are absent altogether from the melilitolites and pyroxenites, a feature also seen in similar rocks from the Gardiner intrusion (Nielson, 1980).

Once again, the Al content is one of the most important variables in distinguishing magnetite and spinel compositions from different groups of rocks (Table 6, Fig. 7). Spinels from the olivine melteigite contain high proportions of $(Fe^{2+},Mg)(Cr,Al)_2O_4$ and most of the analyses have higher Al contents than those shown in Fig. 7. Cr-free magnetite analyses from the olivine melteigite have high Ti contents and high Fe^{2+}#s (defined as $100Fe^{2+}/[Fe^{2+} + Mg]$) and show no ilmenite exsolution. The melilitolite and pyroxenite analyses have the highest spinel contents. In addition, pyroxenite sample C.AG.347 also contains chrome spinel exsolution lamellae within the pyroxene cores.

The melilitolite and pyroxenite magnetite composition fields overlap in Fe^{2+}# and Al space, again suggesting a possible petrogenetic relationship between these two rock types. Although magnetite is rare in the ijolites, it has higher Fe^{2+}# values and lower Al contents than the pyroxenites and melilites, while the Fe^{3+}#s (defined as calculated $100Fe^{3+}/[Fe^{3+} + Fe^{2+}]$) and the abundance of Ti in the pyroxenite, melilitolite and ijolite magnetite analyses are all fairly similar.

The phoscorites and carbonatites have similar magnetite compositions, with relatively high Fe^{2+}#s (>90) and low Ti and low Al contents. Only analyses from the northern-complex pyroxene-calcite carbonatite [sample N.63.4] do not show these characteristics, but overlap the analyses from the northern melilite-bearing samples in Fe^{2+}#, Al and Ti space.

Ilmenite analyses from micro-intergrowth features within magnetite from ijolites, phoscorites, carbonatites and turjite, show very Mg- and Mn-rich compositions, which is common in micro-intergrowth features from magnetite in igneous and metamorphic rocks (Deer *et al.*, 1992). $FeTiO_3$ remains the dominant solid-solution component, but combined pyrophanite

TABLE 6. Selected magnetite and ilmenite compositions from a variety of rock types. Magnetite analyses normalized with 3 cations:4 anions. Ilmenite analyses normalized with 2 cations:3 anions.

Sample	C.AG.347	C.AG.48A		C.IJ.14	C.190.105	TUR II	C.K.7		C.TL.344	C.6.15		C.49.40
Rock type	Pyroxenite	Ol. melteigite		Ijolite	Turjaite	Ultramel.	Phoscorite		Carb.	Carb.		Carb.
Analysis	PT 60	PT 32	PT 62	PT 8	PT 68	PT 4	PT 39	PT 38	PT 68	PT 23	PT 22	PT 43
MgO	3.86	6.39	0.84	0.09	0.81	3.76	1.86	9.67	2.24	1.49	11.57	0.44
MnO	0.66	0.55	0.99	0.63	0.99	1.22	0.75	3.50	0.91	0.28	2.27	0.11
FeO	31.24	28.89	39.05	33.10	33.68	30.41	30.41	29.68	33.23	30.60	27.98	31.53
Fe_2O_3	55.10	35.79	46.72	62.15	59.02	56.57	62.75	1.12	57.06	64.45	1.50	66.94
Al_2O_3	2.89	6.62	0.71	0.14	1.59	2.50	0.08	0.00	0.20	0.18		
V_2O_3	0.11	0.09	0.22	0.18	0.16	0.14	0.46	0.28	0.17	0.29	0.56	0.24
Cr_2O_3	0.10	14.15	0.05				0.17	0.17				
SiO_2		0.11	0.17		0.11	0.22	0.30	0.28	0.67			0.12
TiO_2	6.60	7.27	10.84	3.20	4.51	5.86	2.88	55.75	5.92	2.38	56.61	1.06
Total	100.56	99.86	99.59	99.49	100.87	100.68	99.67	100.45	100.40	99.67	100.49	100.44
Mg	0.209	0.333	0.047	0.005	0.045	0.204	0.105	0.337	0.125	0.085	0.398	0.025
Mn	0.020	0.016	0.032	0.021	0.031	0.038	0.024	0.069	0.029	0.009	0.044	0.004
Fe^{2+}	0.951	0.845	1.236	1.067	1.054	0.927	0.964	0.580	1.038	0.975	0.540	1.006
Fe^{3+}	1.509	0.943	1.330	1.803	1.663	1.551	1.790	0.020	1.604	1.847	0.026	1.923
Al	0.124	0.273	0.032	0.006	0.070	0.108	0.004		0.009	0.008		
V	0.003	0.003	0.007	0.006	0.005	0.004	0.014	0.005	0.005	0.009	0.010	0.007
Cr	0.003	0.392	0.001				0.005	0.001				
Si		0.004	0.006		0.004	0.008	0.011	0.007	0.025			0.005
Ti	0.181	0.191	0.308	0.093	0.127	0.161	0.082	0.980	0.166	0.068	0.982	0.030
Total	3.000	3.000	3.000	3.000	3.000	3.000	3.000	2.000	3.000	3.000	2.000	3.000

Rock type abbreviations: Carb. = melilite carbonatite; Ultramel. = ultramelilitolite
Blank spaces: below detection level

($MnTiO_3$) and geikeilite ($MgTiO_3$) components account for up to 55 mol.%. Ilmenite from the phoscorites and carbonatites is rich in Mg, whereas the ilmenite from one ijolite sample contains no Mg, but significant quantities of Mn.

Perovskite

Two types of perovskite are found at Turiy. The first, normally deep brown, occurs as discrete, fine- to medium-grained crystals with cores which commonly contain many solitary inclusions. The second type occurs as 5–100 μm colourless rims around the edges of magnetite crystals. These rims may be overgrown or replaced by garnet or phlogopite. Such perovskite rims are common in the melilitolites; similar rims have been reported in melilitolites from the Gardiner complex which were attributed to Ti exsolution from magnetite during 're-equilibration' (Nielsen *et al.*, 1997). Perovskite rims have also been reported around Mg-ilmenite grains in kimberlites (Boctor and Boyd, 1979).

Compositional differences exist between the two types of perovskite in the Turiy rocks (Table 7). The individual dark brown crystals are almost pure $CaTiO_3$, with some enrichment in Nb, while the rims contain <10% of the loparite component ($Na\mathit{REE}Ti_2O_6$) as well as latrappite ($Ca_2Fe^{3+}NbO_6$). This is a reversal of the enrichment seen in the Gardiner perovskites, where early perovskite is rich in Nb and *REE*, and the rims are almost pure $CaTiO_3$ (Nielsen, 1980). Figure 8 shows a plot of Na *vs*. [La + Ce] for all Turiy perovskite. The melilitolites generally have atomic [La+Ce] > Na, and the ijolites have atomic [La+Ce] < Na. Perovskites from the melilite-calcite rocks from the northern complex are the most highly enriched in *REE*, and also

TABLE 7. Selected analyses of perovskite from the Turiy rocks. Analyses normalized to 3 anions.

Sample	C.90.29	C.AG.48A	C.IJ.14		C.190.105	E.133.30
Rock type	Pyroxenite	Ol. melt.	Ijolite		Turjaite	Turjaite
Analysis	PT 46	PT 64	PT 27	PT 44	PT 59	PT 45
Nb_2O_5		1.05	6.82	0.78	0.85	1.97
TiO_2	57.10	55.73	47.97	55.36	55.35	52.89
SiO_2		0.06				0.09
Al_2O_3	0.11	0.09	0.10	0.11	0.26	0.13
V_2O_3		0.25	0.37	0.18	0.10	0.13
La_2O_3		0.65	6.95	1.08	0.91	1.21
Ce_2O_3	0.48	1.60	8.35	2.27	2.00	3.00
FeO	1.00	0.84	0.31	1.27	1.54	1.48
MgO						
SrO	0.35				0.37	0.59
CaO	39.73	37.12	16.60	37.15	37.54	35.62
Na_2O	0.11	0.66	5.16	0.66	0.41	0.82
Total	98.88	98.06	92.63	98.86	99.33	97.93
Nb		0.011	0.083	0.008	0.009	0.021
Ti	0.991	0.983	0.967	0.976	0.972	0.953
Si		0.001				0.002
Al	0.003	0.002	0.002	0.003	0.007	0.004
V		0.005	0.008	0.003	0.002	0.002
La		0.006	0.069	0.009	0.008	0.011
Ce	0.004	0.014	0.082	0.019	0.017	0.026
Fe^{2+}	0.019	0.016	0.007	0.025	0.030	0.030
Mg						
Sr	0.005				0.005	0.008
Ca	0.982	0.933	0.477	0.934	0.939	0.915
Na	0.005	0.030	0.268	0.030	0.019	0.038
Total	2.008	2.001	1.963	2.009	2.007	2.010

contain ~8% latrappite. Most of the melilitolite and ijolite samples contain ~4.5% loparite and 1–2% latrappite, although one analysis from urtite sample C.IJ.14 contains 30% loparite, 8% lueshite ($NaNbTiO_3$) and only 48% perovskite.

That many magnetite grains in the melilitolites are surrounded by rims of perovskite (and/or garnet) has implications for the oxygen fugacity of the melt since the isolation of significant quantities of magnetite from the magma will alter its ability to buffer the oxygen fugacity, and hence alter the subsequent crystallization process. Mysen *et al.* (1976) and Dunworth and Wilson (1998) have shown that saturation of a melt in Fe^{3+} is critical to the timing of melilite precipitation in extrusive melilitites. If, however, the growth of the perovskite rims takes place under sub-solidus conditions, the effective 'removal' of magnetite from the system due to its enclosure by perovskite, will have minimal effect on the oxygen fugacity of the remaining magma.

Apatite

The composition of apatite, another ubiquitous mineral at Turiy, again shows systematic variations depending on rock type (Table 8). Le Bas and Handley (1979) described similar findings from East African carbonatites. Typical solid-solution substitutions, which occur on a minor scale, include Sr for Ca, and coupled substitutions such as Ca + P ⇌ *REE* + Si. MnO contents and total *REE* patterns, commonly used to characterize carbonatite apatite chemistry (Hogarth, 1989), are, as yet, not available from the Turiy apatites. Instead, a plot of Sr *vs.* Si content (Fig. 9) can be used to demonstrate variations in apatite composition among the different rock types. Although the concentrations of these two elements in apatite are low, the analyses were reproducible and consistent throughout the duration of the study.

The pyroxenite and melilitolite apatites all have low Sr and variable Si contents, as shown in Fig. 9. The olivine melteigite apatite analyses contain ~0.07 a.p.f.u. of both Si and Sr, while most of the ijolite analyses have Sr > Si. Those apatite analyses from the ijolites with Si > Sr were obtained from an ijolite-melilitolite contact [sample C.ND.500] and a micro-ijolite [sample WKM]. Strontian fluorapatite which contains virtually no Si, but up to 0.42 a.p.f.u. Sr (6.6–8.1 wt.% SrO), is found in the ijolite part of an ijolite-fenite contact sample.

The large cluster of carbonatite and phoscorite analyses with very low Sr and low Si contents were obtained from samples from the central complex, and these show little overlap with analyses from the silicate rocks. The carbonatite analyses with high Si contents (0.12–0.22 a.p.f.u.) and low Sr contents, are from the northern complex carbonatites which either contain melilite or are associated with melilite-

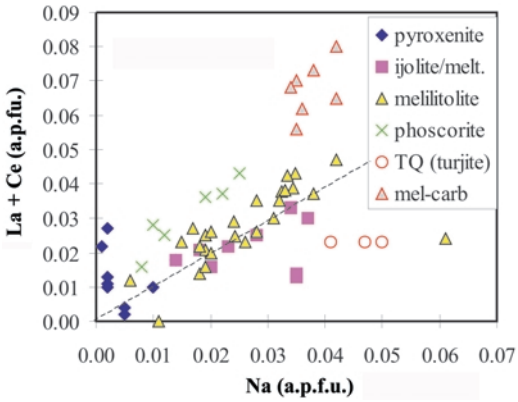

FIG. 8. Perovskite compositions from the Turiy rocks, showing the amount of loparite ($NaRETi_2O_6$) component present. The northern-complex melilite-carbonatite perovskites are additionally enriched in *REE*. Most melilitolite perovskite analyses contain [La + Ce] > Na, while the ijolite perovskite analyses contain Na < [La + Ce].

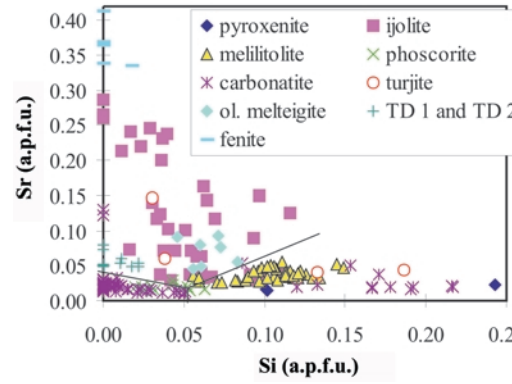

FIG. 9. Apatite analyses from the Turiy rocks. The plot provides a means of dividing the analyses into groups according to the rock type from which they are derived. See main text for further explanation. Sample TD 1 = late-stage fluorite-apatite-carbonate vein, and TD 2 = late-stage aegirine-augite-apatite-ankerite vein, both from the south coast.

TABLE 8. Selected analyses of apatite from the Turiy rocks. Analyses normalized to 13 anions.

Sample	C.AG.347	C.AG.48A	C.IJ.14	C.5.118	TUR 1	C.K.7	C.TL.344	C.54.x	N.64.19	TQ	TD2	Ij/fen
Rock type	Pyroxenite	Ol. melt.	Ijolite	Turjaite	Turjaite	Phosc.	Carb.	Carb.	Carb.	Turjite	Aeg.-ap. vein	Ijolite
Analysis	PT 64	PT 68	PT 6	PT 24	PT 16	PT 52	PT 59	PT 30	PT 65	PT 50	PT 42	PT 70
Na_2O	0.06					0.28	0.13		0.09	0.11		0.05
CaO	53.84	53.12	51.72	55.78	53.15	54.61	55.11	52.74	51.13	54.73	54.57	48.95
SrO	0.44	1.54	5.28	0.56	1.13	0.34	0.27	1.03	0.42	0.81	1.63	8.08
La_2O_3		0.55	0.16		0.53			1.28	1.13	0.34		0.54
Ce_2O_3		1.01	0.24	0.18	0.92			1.82	2.64	0.39	0.14	0.71
Nd_2O_3								0.43	1.17			
SiO_2	2.87	0.86		1.15	1.30	0.75	0.61	1.79	2.49	1.56		
P_2O_5	39.78	40.62	41.47	40.58	40.50	42.10	42.09	39.37	38.34	39.80	41.38	39.69
F	1.92	3.00	1.84	2.97	3.49	2.07	2.58	1.30	2.15	2.90	4.07	4.03
H_2O*	0.86	0.33	0.88	0.37	0.10	0.81	0.57	1.13	0.71	0.39	-0.17	-0.21
O=F	−0.81	−1.26	−0.77	−1.25	−1.47	−0.87	−1.09	−0.55	−0.91	−1.22	−1.71	−1.70
Total	98.97	99.77	100.82	100.34	99.65	100.09	100.27	100.35	99.36	99.81	99.91	100.14
Na	0.010					0.045	0.021		0.015	0.018		0.009
Ca	4.874	4.861	4.729	5.035	4.852	4.889	4.933	4.840	4.757	4.987	4.970	4.621
Sr	0.022	0.076	0.261	0.027	0.056	0.016	0.013	0.051	0.021	0.040	0.081	0.413
La		0.017	0.005		0.017			0.040	0.036	0.011		0.018
Ce		0.032	0.007	0.006	0.029			0.057	0.084	0.012	0.005	0.023
Nd								0.013	0.036			
Si	0.243	0.073	0.000	0.097	0.111	0.063	0.051	0.153	0.216	0.133		
P	2.846	2.937	2.996	2.894	2.921	2.978	2.977	2.855	2.819	2.866	2.978	2.961
F	0.513	0.810	0.497	0.791	0.940	0.547	0.682	0.352	0.591	0.780	1.094	1.123
Total	7.994	7.997	7.999	8.059	7.986	7.992	7.994	8.009	7.985	8.067	8.032	8.043

Rock type abbreviations: Phosc. = phoscorite; Carb. = carbonatite; Aeg.-ap. = aegirine-apatite
Blank spaces: below detection level

bearing rocks. At Turiy the Sr contents of apatite are consistently lower than the Sr contents of co-existing calcite, a feature that is also shown by many African carbonatites (Dawson *et al.*, 1996).

The turjite data points are derived from two samples. Data from sample TU 120A fall close to those from the ijolite samples C.IJ.14 and E.123.106 (two possible candidates for a turjite precursor magma) while turjite sample TQ, which contains quenched relict laths of melilite, has apatite compositions that plot close to those from the melilitolites.

Carbonates

In the carbonatites, calcite occurs in a variety of textures, as described earlier. Dolomite occurs as small rhombs in the phoscorites and forms veins in some of the magnetite-apatite-tetra-ferriphlogopite-rich carbonatites from the central complex. However, dolomite is extremely rare in melilite-bearing carbonatites from the northern complex. The late-stage carbonatites are more enriched in dolomite (up to 50 modal %), while ankerite has only been found in late-stage veins from the south coast [samples TD 1 and TD 2]. MnO contents are <0.25 wt.% in all calcite analyses, <0.4 wt.% in all dolomite analyses and <2.2 wt.% in ankerite from the ankerite-fluorite vein sample TD 1. Zaitsev (1996) showed that Sr enrichment in calcite (~1 wt.% SrO) from the Khibina massif was characteristic of primary calcite, while low Sr contents characterized secondary calcite. Most calcite analyses from the carbonatites and phosocorites at Turiy contain 0.47–0.73 wt.% SrO (Dunworth, 1997). No systematic variation has been found between calcite composition and rock type at Turiy.

Strontianite forms small crystals along grain boundaries in many of the carbonatite and silicate

TABLE 9. Selected analyses of götzenite, stronalsite and banalsite from the Turiy rocks.

Sample	C.AG.122		E.133.30		C.IJ.14
Rock type	Melteigite		Melilitolite		Urtite
Analysis	PT 4		PT 60		PT 51
SiO_2	32.81	SiO_2	38.66	SiO_2	37.02
TiO_2	9.53	Al_2O_3	32.02	TiO_2	0.14
Al_2O_3	0.58	Fe_2O_3	0.37	Al_2O_3	30.15
Ce_2O_3	2.14	MgO	0.05	FeO	0.46
MgO	1.34	SrO	16.49	BaO	22.86
FeO	1.11	CaO	0.51	SrO	0.14
SrO	0.55	Na_2O	10.00	CaO	
CaO	38.96	K_2O		Na_2O	9.35
Na_2O	4.65	Total	98.10	K_2O	0.10
K_2O	0.31			Total	100.22
F	8.55				
O=F	−3.60				
Total	96.93				
Si	1.354	Si	4.011	Si	4.053
Ti	0.296	Al	3.915	Ti	0.011
Al	0.028	Fe^{3+}	0.029	Al	3.891
Ce	0.032	Mg	0.008	Fe^{2+}	0.043
Mg	0.082	Sr	0.992	Ba	0.981
Fe^{2+}	0.038	Ca	0.056	Sr	0.008
Sr	0.013	Na	2.011	Ca	
Ca	1.723	K		Na	1.984
Na	0.372	Total	11.021	K	0.013
K	0.016	O	16	Total	10.989
F^-	1.116	Stronalsite		O	16
Total	3.956			Banalsite	
O	6				
Götzenite					

samples. Trace quantities of Ba and *REE* carbonates have also been found in some of the carbonatites from Turiy, but in insufficient quantities for accurate analysis and identification.

Other minerals

Additional minerals of significance and/or interest are found mostly in trace quantities in a few of the samples; analyses of some of the less common minerals are listed in Table 9.

Cancrinite is abundant in melilitolite sample TUR I and occurs in place of nepheline in accordance with the experimental results of Watkinson and Wyllie (1971) (Dunworth and Bell, 1996).

Banalsite [$Na_2BaAl_4Si_4O_{16}$] occurs along grain boundaries in melteigite sample C.AG.122 and ijolite sample C.IJ.14, whilst stronalsite [$Na_2SrAl_4Si_4O_{16}$], occurs in trace quantities along grain boundaries in the eastern melilitolite sample E.133.30.

Titanite [$CaTiSiO_5$] is limited in its occurrence at Turiy. It is found in pyroxenite, olivine melteigite, turjite and ijolite, and is absent from the melilitolites. Only found in trace quantities, it is fine-grained and shows little compositional variation, although minor Zr substitutions can occur.

Four zirconium minerals were found in the Turiy rocks – zircon, zirsinalite, calzirtite and baddeleyite. Zircon grains are extremely rare in all the samples analysed, mostly found in carbonatites, and all are <20 μm in diameter. One carbonatite contains a 5 μm zircon inclusion in apatite and two of the youngest central massif calcite carbonatites contain trace quantities of zirsinalite [$Na_6(Ca,Mn,Fe)ZrSi_6O_{18}$] and calzirtite [$Ca_2Zr_5Ti_2O_{16}$] along grain boundaries. Baddeleyite and zircon analyses also contain Hf in detectable quantities.

Götzenite $(Ca,Na)_3(Ti,Al)Si_2O_7(F,OH)_2$ was identified, on the basis of its chemical composition, from melteigite sample C.AG.122.

Sulphide phases are found in almost all rock types, and consist primarily of pyrrhotite and chalcopyrite. The greatest abundances occur in the youngest carbonatites and the phoscorites. Sulphide immiscibility textures are found in the latter. An unidentified sulphide phase, [Fe_3CuS_4], was found in melteigite sample C.AG.122, and djerfisherite [$K_6Na(Fe,Cu)_{24}S_{26}Cl$] was found in melilitolite sample TUR II. Both of these samples also contain pyrrhotite.

Discussion

Four questions which arise from the petrological and mineralogical data presented thus far are: (1) Can the mineral chemistry help identify which rock types are petrogenetically related to one another? (2) What factors control the partitioning behaviour of different elements? (3) How do the carbonatite magmas evolve? (4) Can mineral compositions be used to provide estimates of formation temperatures?

Petrogenetic relationships

It can be seen from several of the mineral composition plots that there are compositional similarities between the minerals found in the pyroxenites and melilitolites, as shown by garnet, apatite and magnetite. Such similarities are also seen between the melilitolites and the melilite-bearing carbonatites within the northern massif, as shown by garnet, mica, apatite and magnetite. Similarities are also seen between the apatite, garnet, mica and pyroxene compositions of the olivine melteigite and many of the ijolite samples. Isotopic and geochemical data, along with major and trace element modelling (Dunworth and Bell, 2001), all support the magmatic relationships exhibited by these mineralogical trends, and preclude the derivation of the massif from a single parental magma. The dissimilarity between the central-complex carbonatites and phosocorites and the silicate rocks that has already been shown by the isotope data (Dunworth and Bell, 2001), is also borne out by the mineral chemistry. The parental magmas to the central-complex carbonatites and phoscorites cannot be the same as those that produced the silicate rocks, and the carbonatite and phoscorite parent magmas (or conjugate immiscible silicate liquids) currently remain unknown.

Bell *et al.* (1996) proposed that turjite was produced by the reaction of a carbonatite with an ijolite magma, based on the experimental results of Verwoerd (1978). It is further suggested here that the olivine melteigite pipe from the central complex, the second generation ijolites, (represented by sample C.IJ.14) and the turjite magmas share a petrogenetic relationship based on fractional crystallization of a melteigitic magma and reaction with carbonatite. This relationship may be seen petrographically in Fig. 2(*g*–*j*) and can be reproduced in terms of major-element modelling (Dunworth and Bell, 2001). Figure 2*g*

TABLE 10. Summary of mineralogical differences between the ijolite- and melilitolite-series rocks.

Mineral	Characteristic	Ijolite-series rocks	Melilitolites
Pyroxene	Abundance	15−70%	<4%
	aegirine content	aeg ij > mel.	aeg mel < ijolite
	Tschermak content	Tsch. ij < mel.	Tsch.mel. > ijolite
Garnet	Abundance	5−25%	<4%
	^{vi}Al content	none present	none present
Mica	Abundance	0−12%	2−35%
	^{vi}Al content	none present	always present
	Al:Si and Mg#	ijolite < mel.	mel. > ijolite
Apatite	Si:Sr	Si < Sr	Si > Sr
Magnetite	Abundance	0−7%	3−30%
	Al content	ijolite < mel.	mel. > ijolite

[Note that "always" or "<", ">" are used here to express approximately 90% confidence levels mel. = melilitolite, and Tsch. = $CaTiAl_2O_6$ + $Ca(Fe^{3+}Al)_2SiO_6$ components]

shows olivine co-existing with augite and nepheline in the olivine melteigite. Some of the pyroxene compositions match those of pyroxene enclosed within phlogopite in the urtite sample C.IJ.14 (see Fig. 2*h*), where garnet is abundant. The turjite contains cumulate garnet (shown in Fig. 2*i*) and in Fig. 2*j* the pyroxene is completely replaced by tetra-ferriphlogopite, a reaction relationship commonly seen in alkaline rocks (Brod *et al.*, 2001). The experiments of Verwoerd contained both calciocarbonatite and natrocarbonatite but the absence of natrocarbonatite at Turiy suggests that a Na-rich hydrothermal fluid may be considered as an alternative component in this reaction.

Element partitioning

One of the most obvious features of the mineralogical composition variations is the co-ordination behaviour of Al and Fe^{3+} in minerals such as garnet and mica, and their systematic variation between rock-types (Table 10). This may be due to a combination of three reasons: (1) low Si contents requiring all Al to form ^{iv}Al to fill tetrahedral sites; (2) variable partitioning of Al and Fe^{3+} between tetrahedral and octahedral co-ordination in the host melt; and (3) the timing of Fe^{3+} saturation in the silicate melt.

Major-element whole-rock data (Dunworth and Bell, 2001) show that the SiO_2 content of the melilitolites (35.5−37.5 wt.%) and ijolites (39.2−40.9 wt.%), do not exhibit a direct relationship between whole-rock Si content and the solid-solution behaviour of their constituent minerals described earlier. However, the Al_2O_3/SiO_2 ratios (melilitolites = 0.37−0.44; ijolites = 0.31−0.33) provide better correlation. The abundance of magnetite in the melilitolites and its virtual absence in the ijolites suggest that the proportion of total Fe^{3+} dissolved within the silicate melt is significantly lower in the melilitolites than the ijolites. The relatively high value of the whole-rock Fe_2O_3/Al_2O_3 ratio in the ijolites (0.81−0.89) correlates with the high proportion of $^{iv}Fe^{3+}$ seen in the ijolite garnets and micas. Thus, it seems that a high Al/Si ratio in the melilitolite melts (Poe *et al.*, 1992), and high Fe^{3+} activity within the ijolite melts may dominate the Al and Fe^{3+} site-partitioning behaviour and solid-solution variations seen in silicate phases such as garnet and mica. The low Si content of the melilitolites causes early silicate melt saturation in network-forming cations such as Fe^{3+}, Ti and P, initiating the crystallization of Si-free phases such as magnetite, perovskite and apatite. The higher Si-content of the ijolites allows continued solution of Fe^{3+} and Ti in the silicate melt, initiating the crystallization of significant amounts of Ti and Fe^{3+}-bearing silicate phases in most of the samples. Mysen *et al.* (1976) and Dunworth and Wilson (1998) have also shown that the saturation of a melt in Fe^{3+} is critical to the timing of melilite formation in extrusive melilitites, and this may

also be a key factor in the timing of intrusive melilite crystallization.

Another way to move Al out of tetrahedral coordination within a silicate melt is to add volatiles (e.g. H_2O, CO_2 or F) which preferentially form complexes with Na, and prevent the formation of [NaAl] tetrahedra linked to Si, hence leaving Al free to form ^{vi}Al instead (Mysen *et al.*, 1980; Mysen and Virgo, 1980, 1985). If these silicate-melt results can be extrapolated to the melilitolite magmas, then it would suggest that the melts were particularly enriched in dissolved volatiles at the point of crystallization, which is supported by the high abundance of minerals such as phlogopite and calcite in these melilite-bearing samples.

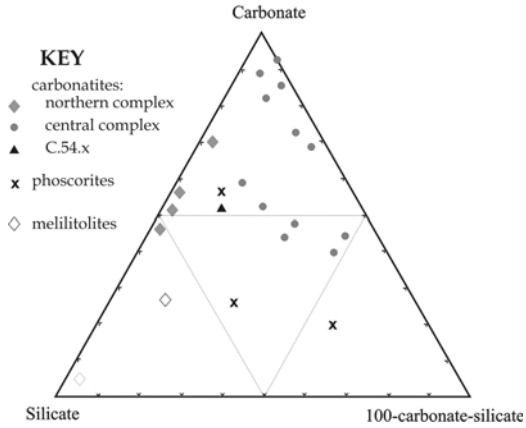

FIG. 10. Ternary diagram based on the modal mineralogy of the carbonatites and phoscorites. The minerals representing the [100-silicate-carbonate] apex are dominated by apatite and magnetite.

Carbonatite evolution

Some interesting mineralogical variations in the modal mineralogy of the Turiy carbonatites and phoscorites, are summarized in Fig. 10. It can be seen that the northern carbonatites are rich in silicate and carbonate phases and relatively poor in non-silicate, non-carbonate phases (e.g. magnetite and apatite). Figure 10 also shows that one group of central carbonatite samples is carbonate-rich (including two dolomite-rich samples), and contains <10% silicate phases, and <30% non-silicate, non-carbonate phases. An apparent compositional gap, which may be due to inadequate sampling, gives way to another cluster of central carbonatite points located between 40 and 58% carbonate. Ignoring the natrolite-rich sample C.54.x, this latter group contains <30% silicate phases but is rich in 'non-silicate, non-carbonate phases' (17–50%). The phoscorites have also been plotted in Fig. 10, along with data from the calcite melilitolite sample N.64.18m.

Measured and estimated major element data (Dunworth, 1997) suggest that none of the central-complex massif carbonatites contains >10% SiO_2, although the northern massif carbonatite samples are estimated to contain ~11–25% SiO_2, some of which may have been incorporated as a result of crustal contamination (Dunworth and Bell, 2001).

It should be noted that those central complex carbonatites with <20% '100-silicate-carbonate' phases in Fig. 10, i.e. low magnetite and apatite contents, contain micas with Mg# <90. This may be due to low f_{O_2} or Fe undersaturation of the melt preventing the crystallization of magnetite, thus creating a lower Mg# in the melt and in the ferromagnesian minerals crystallizing from it. The fact that the mica Mg# is inversely proportional to magnetite + apatite content in these samples suggests that the mineral phases in these carbonatites crystallized in equilibrium with each other, and that these samples therefore represent a closed-system melt and not open-system cumulates, as is also borne out by mineral-separate isotope data (Dunworth and Bell, 2001).

An evolutionary model for the carbonatites, based on the major element chemistry of the Turiy carbonatites along with the chemical and textural characteristics of their constituent minerals, can now be outlined. The most SiO_2-rich carbonatites are those from the northern complex. Several of these samples contain ^{vi}Al-bearing garnet, mica and abundant pyroxene. Where melilite and monticellite are present, apatite and mica are rare. The minerals precipitating out of the melt had high Al/Si ratios, moderately high Mg#s, and the melt was saturated in carbonate which precipitated calcite but not dolomite. The f_{O_2} and/or Fe contents are too low to produce abundant magnetite. There is no clear age-relationship between these and the central-complex carbonatites, but Kapustin (1980) has suggested, on the basis of modal mineralogy, that such carbonatites are normally early carbonatites. Mineralogical and geochemical data (Dunworth, 1997) suggest that these carbonatites are, in fact, related to the melilitolites.

The central-complex carbonatites appear to be more evolved, according to the mineralogical

model of Kapustin (1980). The four essential minerals in most of the central complex carbonatites (and phoscorites) are calcite, apatite, magnetite and tetra-ferriphlogopite. Amphibole and pyroxene are rare, while melilite, garnet and monticellite are absent. Aluminium reaches minimal concentrations in the silicate minerals and in magnetite, and the bulk-rock Si contents are also lower than in the northern carbonatites. The earliest carbonatites in the central complex, according to field evidence (Bulakh and Ivanikov, 1984), contain rare pyroxene along with magnetite and apatite. Later carbonatites contain mica instead of pyroxene (similar to the progression seen in ijolite sample C.IJ.14), and Mg# increases as Fe^{2+} is used up in the production of magnetite (Brod *et al.*, 2001) and little Fe^{2+} is available for entry into the silicate phases. The preferential combination of CO_3^{2-} anions with Ca^{2+} (Holloway *et al.*, 1976; Mysen and Virgo, 1980; Dalton and Presnall, 1997) leaves the melts saturated in Mg and Si. It should be noted that Na cannot partition into any of the four dominant minerals phases at this time, and that the pyroxene in the earlier carbonatites also has low Na contents. Whether the melts were already depleted in Na due to earlier fractional crystallization and fenitization, or whether Na remained in solution at this point, is currently unclear. The saturation of the melt in Mg, and exhaustion of available Si and K, causes the cessation of mica crystallization with subsequent precipitation of dolomite while magnetite is still crystallizing. Thus, the mineral assemblage evolves, in general, from calcite + pyroxene + magnetite + apatite ± amphibole ± mica, to calcite + dolomite + magnetite + apatite + mica. The later, carbonate-rich samples become increasingly dolomite-rich and are increasingly poor in silicate minerals, although magnetite and apatite contents can remain high. The most evolved samples contain equal amounts of calcite and dolomite, along with small quantities of apatite and sulphides, but no silicate phases or magnetite.

Geothermometry

The apatite-biotite geothermometer of Ludington (1978), based on mica composition, and F and OH contents of both phases, has been used to estimate apatite-biotite equilibration temperatures in 23 samples covering the entire suite of rock types seen in the massif. Overall average values from each sample range from 540–950ºC. The ranges for each sample type (number of samples in brackets) are: (a): melteigite–ijolite series (4) = 775–843ºC; (b) melilitolites (5) = 538–798ºC; (c) phoscorites (2) = 658–762ºC; and (d) carbonatites (10) = 664–950ºC. Evaluating textural (and hence chemical) equilibrium, as well as the extent of subsolidus re-equilibration, in the Turiy samples is a difficult task, and thus the errors associated with these temperature estimates are difficult to quantify. However, the dominance of temperatures in the 650–800ºC range give estimates which may provide the basis for future work.

Conclusions

The variations in the mineralogical data from the Turiy massif show that closed-system fractional crystallization of a single batch of magma cannot be responsible for producing the wide variation in rock types seen within the Turiy massif. Petrographic features of many of the silicate and carbonate samples, which include banding, crystal accumulation, the presence of veins and mineral overgrowths, are all indicative of open-system crystallization.

Mineral compositions can, however, be correlated with the host rock type. Systematic variations in mineral compositions are seen in apatite, garnet, melilite, mica, nepheline, magnetite, perovskite and pyroxene. Minerals from the melilitolites contain relatively high quantites of Al (magnetite), Al in octahedral co-ordination (garnet, mica), high quantities of Tschermak components (pyroxene), high *REE* contents (apatite, perovskite) and Si > Sr in apatite compositions. Mineral compositions of pyroxene, apatite, perovskite and magnetite from the pyroxenites share many similarities with those from the melilitolites, and the two rock types are believed to be related through fractional crystallization.

Petrographic and mineral composition similarities are also seen between the olivine melteigite, ijolite and turjite samples. These include the presence of $^{iv}Fe^{3+}$ in mica and garnet compositions, Sr>Si in apatite compositions, lower Tschermak and higher aegirine contents in pyroxene compositions relative to those seen in the melilitolites and pyroxenites. The *REE* contents in the ijolite apatite and perovskite compositions are lower than those of the melilitolites and pyroxenites.

The mineralogy, petrology and isotope chemistry of the phoscorites suggest that they are magmatic liquids, and not cumulates from a carbonatite magma. The phoscorites are coarse-grained and contain segregations of specific minerals, either as clusters, e.g. phlogopite, or as veins, e.g. apatite.

The mineral compositions of the northern complex carbonatites, which are relatively rich in silicate minerals and poor in magnetite and apatite, suggest that these carbonatites are related to the melilitolites.

Mica from the central complex carbonatites and phoscorites are dominated by high-Mg tetra-ferriphlogopite, while apatite compositions from the two rock types have low Si and Sr contents. A clear evolutionary trend within the central complex carbonatites shows a transition from pyroxene-calcite carbonatites to mica-magnetite-apatite-calcite carbonatites, and finally dolomite-calcite carbonatites. A parental magma for the central complex carbonatites has not yet been identified.

Apatite-mica geothermometry from twenty-four silicate-rock and carbonatite samples indicates that these two mineral phases last equilibrated at temperatures ranging from 540–950ºC, with most values lying between 650 and 800ºC.

Acknowledgements

The authors would like to thank Andrei Bulakh, Valeriy Ivanikov and colleagues at the University of Saint Petersburg for leading fieldwork excursions to the Turiy Peninsula in 1991 (KB) and 1995 (EAD), and for facilitating additional access to the Saint Petersburg sample collections. Thanks also to Annett Briggs and John Everest for sample preparation, George Dix for use of the cathodoluminesence unit, Scott Ercit, Bob Gault and their colleagues at the CMN for assistance with the microprobe analyses and mineral identification, and Peter Jones (Carleton) for assistance with the SEM. Scott Ercit is also thanked for providing the FORMULA and MICA mineral calculation programs. Alan Woolley and Anatoly Zaitsev are thanked for their constructive comments on an earlier version of the manuscript. This work was funded by NSERC grant A7813 to K. Bell.

References

Abrecht, J. and Hewitt, D.A. (1988) Experimental evidence on the substitution of Ti in biotite. *American Mineralogist*, **73**, 1273–1284

Araújo, D.P. (1996) *Metassomatismo no complexo carbonatítico Catalão-I: implicações para a copmosição do magma carbonatítico e para o metassomatism carbonatítico no manto superior*. Unpublished MSc thesis, University of Brasilia, Brasil.

Beliankin, D.S. and Kupletskii, B.M. (1924) Rocks and mineral resources of the northern shore and islands of the Gulf of Kandalaksha. *Trudy Severnoi Nauchnoprormyshlennoi ekspedicii*, **28**, 3–76 (in Russian).

Bell, K., Dunworth, E.A., Bulakh A.G. and Ivanikov, V.V. (1996) Alkalic rocks of the Turiy Massif, Kola Peninsula, including type-locality turjaite and turjite: a review. *The Canadian Mineralogist*, **34**, 265–280

Boctor, N.Z. and Boyd, F.R. (1979) Distribution of the rare earth elements in perovskites from kimberlites. *Carnegie Institute of Washington Annual Report from the Director of the Geophysical Laboratory*, **1978–1979**, 572–574

Borodin, L.S. (1963) Perovskite in ultrabasic rocks of the Afrikanda massif and some problems as to the origin of this massif. *Trudy*, IMGRE, **15** (in Russian).

Brod, J.A., Gaspar, J.C., de Araújo, D.P., Gibson, S.A., Thompson, R.N. and Junqueira-Brod, T.C. (2001) Phlogopite and tetra-ferriphlogopite from Brazilian carbonatite complexes: petrogenetic constraints and implications for mineral-chemistry systematics. *Journal of Asian Sciences*, **19**, 265–296

Buddington, A.F and Lindsley, D.H. (1964) Iron-titanium oxide minerals and synthetic equivalents. *Journal of Petrology*, **5**, 310–357

Bulakh, A.G. and Ivanikov, V.V. (1984) *The Problems of Mineralogy and Petrology of Carbonatites*. Leningrad University Publishing House, Saint Petersburg, 240 pp. (in Russian)

Bulakh, A.G. and Ivanikov, V.V. (1996) Carbonatites of the Turiy Peninsula, Kola: role of magmatism and of metasomatism. *The Canadian Mineralogist*, **34**, 403–409

Dalton, J.A. and Presnall, D.C. (1997) Phase relations in the system CaO-MgO-Al_2O_3-SiO_2-CO_2 from 3.0 to 7.0 GPa: carbonatites, kimberlites and carbonatite-kimberlite relations. *GAC/MAC Annual Meeting, Ottawa, Canada*, *Abstracts volume*, A34.

Dawson, J.B., Steele, I.M., Smith, J.V. and Rivers, M.L. (1996) Minor and trace element chemistry of carbonates, apatites and magnetites in some African carbonatites. *Mineralogical Magazine*, **60**, 415–425

Deer, W.A., Howie, R.A. and Zussman, J. (1986) *Disilicates and Ring Silicates, Vol. 1B.* Longman, Harlow, Essex, UK, 629 pp.

Deer, W.A., Howie, R.A. and Zussman, J. (1992) *An Introduction to the Rock-forming Minerals*.

Longman Scientific & Technical, Harlow, Essex, 696 pp.

Dunworth, E.A. (1997) *The Turiy Massif, Kola Peninsula, Russia: Open-system disequilibrium*. Unpublished PhD thesis, Carleton University, Ottawa, Canada, 508 pp.

Dunworth, E.A. and Bell, K. (1998) Melilitolites: a new scheme of classification *The Canadian Mineralogist*, **36**, 895–903.

Dunworth, E.A. and Bell, K. (2001) The Turiy Massif, Kola Peninsula, Russia: isotopic and geochemical evidence for multi-source evolution. *Journal of Petrology*, **42**, 377–405.

Dunworth, E.A. and Wilson, M. (1998) Olivine melilitites of the SW German Tertiary Volcanic Province: mineralogy and petrogenesis. *Journal of Petrology*, **39**, 1805–1836.

Foley, S.F. (1989) Experimental constraints on phlogopite chemistry in lamproites: 1. The effect of water activity and oxygen fugacity. *European Journal of Mineralogy*, **1**, 411–426.

Foley, S.F. (1990) Experimental constraints on phlogopite chemistry in lamproites: 2. Effect of pressure-temperature variations. *European Journal of Mineralogy*, **2**, 327–341.

Gaspar, J.C. and Wylie, P. (1987) The phlogopites from the Jacupiranga carbonatite intrusions. *Mineralogy and Petrology*, **36**, 121–134

Henderson, C.M.B. and Foland, K.A. (1996) Ba- and Ti-rich primary biotite from the Brome alkaline igneous complex, Monteregian Hills, Quebec: mechanisms of substitution. *The Canadian Mineralogist*, **34**, 1241–1252.

Hogarth, D.D. (1989) Pyrochlore, apatite and amphibole: distinctive minerals in carbonatite. Pp. 105–148 in: *Carbonatites, Genesis and Evolution* (K. Bell, editor). Unwin Hyman, London.

Hogarth, D.D. (1997) Mineralogy of leucite-bearing dykes from Napoleon Bay, Baffin Island: multistage Proterozoic lamproites. *The Canadian Mineralogist*, **35**, 53–78.

Holloway, J.R., Mysen, B.O. and Eggler, D.H. (1976) The solubility of CO_2 in liquids on the join CaO-MgO-SiO_2-CO_2. *Carnegie Institute of Washington Yearbook*, **75**, 626–631.

Kapustin, Y.L. (1980) *Mineralogy of Carbonatites*. Amerind Publishing Corporation, New Delhi, 259 pp.

Kogarko, L.N. (1987) Alkaline rocks of the eastern part of the Baltic Shield (Kola Peninsula). Pp. 531–544 in: *Alkaline Igneous Rocks* (J.G. Fitton and B.G.J. Upton, editors). Geological Society Special Publication, **30**. Blackwell Scientific Publications, Oxford, UK.

Kogarko, L.N., Kononova, V.A., Orlova, M.P. and Woolley, A.R. (1995) *Alkaline Rocks and Carbonatites of the World. Part 2: Former USSR*. Chapman & Hall, London, 232 pp.

Kramm, U., Kogarko, L.N., Kononova, V.A. and Vartiainen, H. (1993) The Kola Alkaline Province of the CIS and Finland: Precise Rb-Sr ages define 380–360 Ma age range for all magmatism. *Lithos*, **30**, 33–44.

Kukharenko, A.A., Orlova, M.P., Bulakh, A.G., Bagdasarov, E.A., Rimskaya-Korsakova, O.M., Nefedov, E.I., Illinskiy, G.A., Sergeev, A.S. and Abakumova, N.B. (1965) *The Caledonian Ultramafic Alkalic and Carbonatitic Complexes of the Kola Peninsula and Northern Karelia*. Nedra, Moscow, 772 pp. (in Russian)

Lattard, D. (1995) Experimental evidence for the exsolution of ilmenite from titaniferous spinel. *American Mineralogist*, **80**, 968–981.

Leake, B. (1978) Nomenclature of amphiboles. *The Canadian Mineralogist*, **16**, 501–520.

Le Bas, M.J. and Handley, C.D. (1979) Variations in apatite composition in ijolitic and carbonatitic igneous rocks. *Nature*, **279**, 54–56.

Le Maitre, R.W. (editor) (1989) *A Classification of Igneous Rocks and Glossary of Terms*. Blackwell Scientific Publications, Oxford, UK. 193 pp.

Locock, A., Luth, R.W., Cavell, R.G., Smith, D.G.W. and Duke, M.J.M. (1995) Spectroscopy of the cation distribution in the schorlomite species of garnet. *American Mineralogist*, **80**, 27–38.

Ludington, S. (1978) The biotite-apatite geothermometer revisited. *American Mineralogist*, **63**, 551–553.

Mysen, B.O. and Virgo, D. (1980) Solubility mechanisms of carbon dioxide in silicate melts: a Raman spectroscopic study. *American Mineralogist*, **65**, 885–899.

Mysen, B.O. and Virgo, D. (1985) Interaction between fluorine and silica in quenched melts on the joins SiO_2-AlF_3 and SiO-NaF determined by Raman spectroscopy. *Physics and Chemistry of Minerals*, **12**, 77–85.

Mysen, B.O., Eggler, D.H., Seitz, M.G. and Holloway, J.R. (1976) Carbon dioxide in silicate melts and crystals. Part 1, Solubility measurements. *American Journal of Science*, **276**, 455–475

Mysen, B.O., Virgo, D., Harrison, W.J. and Scarfe, C.M. (1980) Solubility mechanisms of H_2O in silicate melts at high pressures and termperatures: a Raman spectroscopic study. *American Mineralogist*, **65**, 900–914.

Nickel, E.H. and Nichols, M.C. (1991) *Mineral Reference Manual*. Van Nostrand Reinhold, New York, 248 pp.

Nielsen, T.F.D. (1980) The petrology of a melilitolite, melteigite, carbonatite and syenite ring dike system, in the Gardiner complex, East Greenland. *Lithos*, **13**,

181–197.

Nielsen, T.F.D., Solovova, I.P. and Veksler, I.V. (1997) Parental melts of melilitolite and origin of alkaline carbonatite: Evidence from crystallised melt inclusions, Gardiner complex. *Contributions to Mineralogy and Petrology*, **126**, 331–344.

Poe, B.T., McMillan, P.F., Angell, C.A. and Sato, R.K. (1992) Al and Si co-ordination in SiO_2-Al_2O_3 glasses and liquids: A study by NMR and IR spectroscopy and MD simulations. *Chemical Geology*, **96**, 333–349.

Ramsay, W. (1921) En melilitforande djupbergart fran Turiy pa sydsidan av Kolahalvon. *Geologiska Föreningens i Stockholm. Förhandlingar*, **43**.

Rimskaya-Korsakova, O.M. and Sokolova, E.P. (1964) On iron-magnesium mica with reverse scheme of absorption. *Zapiski Vsesoyuznogo Mineralogicheskogo Obshchestva*, **93**, 411–423 (in Russian).

Ronenson, B.M., Afanas'vey, B.V. and Levin, V.Y. (1981) Turjaite parageneses of Tur'ya Peninsula. *International Geology Review*, **23**, 535–543.

Treiman, A.H. and Essene, E.J. (1985) The Oka carbonatite complex, Quebec: geology and evidence for silicate-liquid immiscibility. *American Mineralogist*, **70**, 1101–1113.

Verwoerd, V.I. (1978) Liquid immiscibility and the carbonatite–ijolite relationship: preliminary data on the join $NaFe^{3+}Si_2O_6$–$CaCO_3$ and related compositions. *Carnegie Institute of Washington Yearbook*, **77**, 767–774.

Watkinson, D.H. and Wyllie, P.J. (1971) Experimental study of the composition join $NaAlSiO_4$–$CaCO_3$–H_2O and the genesis of alkalic rock-carbonatite complexes. *Journal of Petrology*, **12**, 357–378.

Zaitsev, A.N. (1996) Rhombohedral carbonates from carbonatites of the Khibina Massif, Kola Peninsula, Russia. *The Canadian Mineralogist*, **34**, 453–468.

Zaitsev, A. and Bell, K. (1995) Sr and Nd isotope data of apatite, calcite and dolomite as indicators of source, and the relationships of phoscorites and carbonatites from the Kovdor massif, Kola Peninsula, Russia. *Contributions to Mineralogy and Petrology*, **121**, 324–335.

Zhang, M., Suddaby, P., Thompson, R.N. and Dungan, M.A. (1993) Barian-titanian phlogopite from potassic lavas in NE China: chemical substitution and paragenesis. *American Mineralogist*, **78**, 1056–1065.

[*Manuscript received 9 August 2002: revised 28 January 2003*]